Separation and Purification Technology 354 (2025) 129112

Contents lists available at ScienceDirect

Separation and Purification Technology

journal homepage: www.elsevier.com/locate/seppur

Silica aerogels modified with vinyl, epoxide, methacrylate moieties for the removal of ciprofloxacin by adsorption from water

Selay Sert Çok [a,b], Fatoş Koç [a,c], Adél Len [b,d], László Almásy [b], Zoltán Dudás [b,*]

[a] Ege University, Faculty of Engineering, Department of Chemical Engineering, 35100 Bornova, İzmir, Turkey
[b] HUN-REN Centre for Energy Research, Neutron Spectroscopy Department, 1121 Budapest, Konkoly-Thege 29-33, Hungary
[c] Ege University, Graduate School of Natural and Applied Sciences, Chemical Engineering Department, 35100 İzmir, Turkey
[d] University of Pécs, Faculty of Engineering and Information Technology, 7624 Pécs, Boszorkány str. 2, Hungary

ARTICLE INFO

Keywords:
Functional silica aerogels
Ciprofloxacin
Antibiotic
Adsorption
Structure–activity relationship

ABSTRACT

Water pollution caused by antibiotic effluents, particularly ciprofloxacin is a growing environmental concern. To address this problem, silica aerogels containing vinyl, epoxide, or methacrylate organic functionalities were synthesized through facile sol–gel synthesis under ambient conditions and employed as ciprofloxacin adsorbents in this study. The physicochemical and structural features of the materials were characterized using conventional and complementary techniques. Structural characterization confirmed the successful chemical functionalization of the silica surface for all samples. Similar to the pristine aerogel, the vinyl-functionalized aerogel displayed a typical mesoporous network, whereas epoxide and methacrylate functionalization caused dominantly macroporous structures. Batchwise sorption experiments were performed under different operating conditions. The results of the equilibrium and kinetic adsorption studies showed excellent alignment with the Langmuir isotherm and pseudo-second-order kinetic models, respectively. Under optimum conditions (C_0 = 100 mg/L, m_{ads}/V_{soln} = 0.5, pH=6, t = 90 min), the adsorption capacities of ciprofloxacin onto vinyl, epoxide, and methacrylate-modified aerogels were 62.7, 45.8 and 47.8 mg/g, respectively. Despite of the differences at micro- meso- and macrostructure level, obtaining similar adsorptive performances confirms that mechanism of sorption is not only relied on pore filling but also controlled by molecular interactions. The adsorbents also exhibited repetable sorption performance for at least six cycles.

1. Introduction

The residuals of pharmaceutically active compounds (PAC) in aquatic environments have recently been considered alarming pollutants because of their ever-increasing use and long-term hazardous effects [1,2]. Among PAC, the quinolone class of antibiotics with low volatility, non-biodegradability, and high eco-toxicity are of primary environmental concern because of their widespread use in human or veterinary medicine, agriculture, and their common detection in water bodies, including surface waters, groundwater, and even drinking water [3–5]. More specifically, ciprofloxacin (CIP), the most prescribed second-generation fluoroquinolone antibiotic, is one of the top pharmaceutical pollutants, and its removal is a high priority for preventing bioaccumulation in ecosystems [6]. The presence of residual CIP in water, even at low concentrations, can trigger the development of antibiotic-resistant genes, causing a serious threat to both aquatic life and human health [7].

To date, many water treatment techniques, including membrane separation [8], advanced oxidation [9], photocatalytic degradation [10,11], ion exchange [12], and adsorption [13–15], have been tested to remove CIP from aquatic media. Considering its ease of operation and scalability, relatively low operational cost, small environmental footprint, and high efficiency, adsorption has generally been accepted as a more convenient technique compared to other methods [16]. Current research has proved that, numerous adsorbents, such as carbon-based materials [17,18], silica-based materials [16,19–21], polymers, resins [22], metal–organic frameworks[23], clays [24], and zeolites [25] have been tested for ciprofloxacin adsorption from water. Among silica-based adsorbents, generally ordered mesoporous silica structures and their composites have been studied for antibiotic removal applications

* Corresponding author.
E-mail addresses: selay.sert@ege.edu.tr (S. Sert Çok), fatoskoc@outlook.com (F. Koç), len.adel@ek.hun-ren.hu (A. Len), almasy.laszlo@ek.hun-ren.hu (L. Almásy), dudas.zoltan@ek.hun-ren.hu (Z. Dudás).

https://doi.org/10.1016/j.seppur.2024.129112
Received 18 June 2024; Received in revised form 24 July 2024; Accepted 4 August 2024
Available online 5 August 2024

[26–28]. On the other hand, amorphous silica structures such as aerogels and xerogels also serve as a viable alternative adsorbent for such applications owing to their very low density, high porosity, high apparent surface area, tunable pore and particle sizes, pore accessibility, adaptable surface properties and ease of functionalization [6].

The use of silica aerogels has been widely reported and proven to be effective in separation processes, particularly for the removal of oil, heavy metals, and organic pollutants [29–32]. However, only a limited number of studies have utilized these superior materials for the removal of antibiotics, particularly CIP, from water [3,6,33]. Recently, Guzelkaya et al. in their study, synthesized a silica xerogel adsorbent from volcanic tuff to evaluate its performance on CIP removal from aqueous solutions and found the maximum adsorption capacity as 24.45 mg/g [6]. Mohseni–Bandpei et al. prepared an amine modified pumice–derived silica aerogel to remove cefixime from water and reported the obtained capacity as 27.43 mg/g [2]. In another study by the same authors, amino functionalization was once again employed through a post-grafting method on pumiced derived silica aerogels to remove ibuprofen yielding a maximum ibuprofen uptake of 39.95 mg/g [34]. Lamy-Mendes et al. also investigated the impact of amino functionalization on carbon nanotubes/silica aerogel composites for the amoxicillin removal from water, achieving the highest adsorption capacity recorded as 19.5 mg/g [35].

As a conclusion drawn from previous studies, it is evident that regardless of the specific pharmaceutical pollutant targeted, functionalization of silica aerogels is a viable strategy for improving the adsorptive capacity towards antibiotics. Electrostatic interactions, hydrogen bonding, π–π interactions, pore diffusion, and hydrophobic interactions are the main mechanisms of CIP adsorption. The interactions between the silica surface and the organic pollutant moieties can be enhanced by simply altering the surface chemistry and surface charge characteristics of the adsorbent. Usually, owing to the abundance of surface hydroxyl groups on the silica structures, pristine silica aerogels possess negatively charged surface groups. These groups are primarily convenient for the adsorption of electron-deficient molecules such as neutral and cationic compounds [2]. However, through appropriate surface modification, silica can also effectively capture anionic moieties. Furthermore, in addition to the surface properties, the uptake is highly affected by the pore characteristics, including pore size distributions, pore accessibility, and interconnectivity. These characteristics as well as the surface properties can be easily adjusted by incorporating different functionalities into the silica skeleton.

To customize the silica surface to adsorb antibiotics, the majority of studies have applied amine functionalization owing to the nucleophilicity of NH_2 groups in aqueous media. Most of these studies involved amine functionalization via a post-grafting method [34,36,37]. Apart from amine functionalization, there is hardly any study in literature that considers other organic functionalities on silica-based materials for capturing CIP molecules from aqueous solutions. Only in one study, Hongasawat et al., reported on superparamagnetic hexagonal mesoporous silica adsorbents functionalized with 3-aminopropyltriethoxysiliane, 4-(triethoxysilyl) butyronitrile, 3-mercaptopropyltriethoxysilane, phenyltrimethoxysilane, and n-octyldimetholchlorosilane via a post grafting approach for the CIP removal and stated that dispersing superparamagnetic iron oxide particles together with the incorporation of phenyl functional groups has yielded an enhanced adsorption capacities and fast equilibrium time [38]. However, tedious synthesis conditions and complicated modification steps make it necessary to be in endeavor on developing more facile modification strategies for silica functionalization.

Therefore, in this study, the authors aimed to address the influence of various organic group substitutions on the design of the chemical and morphological structures of silica aerogels and how they will eventually impact their CIP adsorption ability. For this purpose, vinyl, epoxide, and methacrylate substituents were incorporated into the silica network using a facile one-pot sol–gel synthesis under ambient conditions. Under these conditions, vinyltrimethoxysilane (VTMS), 3-Glycidyloxypropyltrimethoxysilane (GPTMS), and 3-(trimethoxysilyl)propyl methacrylate (TMSPM) precursors were employed in a mixture of classical silicon alkoxide (tetraethylorthosilicate) and methylfunctional silane (methyltriethoxysilane, MTES) through co-gelation, and the wet gels were dried by evaporative drying. Throughout this study, the obtained materials were called aerogels, as they displayed strikingly similar characteristics to their supercritically dried counterparts. The variations caused by different functional groups on the macro-, meso-, and microstructural features of the synthesized adsorbents were monitored using FTIR, SEM, N_2 Sorption, ^{29}Si-MAS-NMR, ^{13}C-CP MAS NMR, and SAXS analyses. In order to test the effectiveness of the synthesized adsorbents, batch sorption experiments were conducted to remove CIP molecules from water. The underlying adsorption mechanisms were investigated using equilibrium and kinetic studies. The change in CIP adsorption efficiency was evaluated depending on various operating conditions, such as initial CIP concentration, adsorbent dosage, pH, and contact time. The optimal conditions that yielded the maximum sorption capacities were determined. The repeatable use of the synthesized adsorbents was also assessed using cyclic adsorption–desorption tests.

To the best of the authors' knowledge, this work represents the first attempt to explore the utilization of silica aerogels with organic functionalities as potential antibiotic adsorbents. Therefore, the results of this study provide guidance for developing functional silica-based adsorbents to remove pharmaceutical pollutants from aqueous media for environmental remediation purposes in the future.

2. Materials and methods

2.1. Materials

In this study, vinyltrimethoxysilane (VTMS, 98 %), 3-Glycidyloxypropyltrimethoxysilane (GPTMS, 98 %), 3-(trimethoxysilyl)propyl methacrylate (TMSPM, 98 %), methyltriethoxysilane (MTES, 99 %), and tetraethyl orthosilicate (TEOS, 99 %) were used as silica precursors. Analytical grade ethanol, n-hexane, and distilled water were used as solvents. Ammonium hydroxide was chosen as the base catalyst, and HCI was used as the eluent in the desorption studies. 1-Cyclopropyl-6-fluoro-4-oxo-7-(piperazin-1-yl)-1,4-dihydroquinoline-3-carboxylic acid (CIP, 98 %) was selected as the target antibiotic. The chemicals were supplied by Merck and were used without further purification.

2.2. Method

Functional silica aerogel adsorbents (S-VTMS, S-GPTMS, and S-TMSPM) were synthesized using a one-step sol–gel method under ambient conditions. In a typical synthesis, the functional organosilanes were mixed thoroughly with TEOS and MTES for 5 min. To initiate the hydrolysis reactions, ethanol and water were added to the mixture and without the addition of any acid catalyst, the solutions were hydrolyzed for 16 h at 25 °C. The molar ratio of total Si/ethanol/water was kept constant at 1/10/20, whereas the molar ratio of the silanes was set to 3/1/6 for organosilane (VTMS, GPTMS, or TMSPM)/MTES/TEOS. Subsequently, to accelerate the condensation reactions, 10 M NH_4OH solution was added dropwise to the obtained mixture until the pH of the sols reached 7. The sols were completely gelated within 1 h and the obtained gels were aged in molds for 12 h. After aging, the wet gels were washed with ethanol and n-hexane for 12 h at 25 °C subsequently to remove the residuals. Finally, the aerogels were dried in an oven at 70 °C overnight and at 110 °C for 2 h. For comparison, a bare silica aerogel (S-BARE SILICA) comprising only TEOS was also synthesized using a similar procedure by keeping the total Si/solvent ratio similar to that in the series. The synthesis pathway and basic characteristics of the reference sample are presented in the Supplementary File (Fig. S2 and Table S1).

2.3. Characterization

The impact of the substitution of different organic functionalities to silica network on the physicochemical and microstructural properties of the aerogels was assessed by complementary combinations of various characterizations. FTIR and ^{29}Si-MAS NMR analyses were employed to identify the chemical composition and degree of functionality of the synthesized aerogels. FTIR spectra of the samples were collected on a PERKIN ELMER Spectrum-100 FTIR analyzer between the wavelength range of 600–4000 cm^{-1}. ^{29}Si-MAS NMR and 13C-CP-MAS-NMR spectra were obtained using a magic-angle spinning (MAS) spectrometer (Bruker Superconducting FT. NMR Spectrometer Avance TM spectrometer) operating at a spinning rate of 8500 Hz with a 4 mm MAS probe at 25 °C.

The textural properties of the adsorbents were evaluated by N_2 sorption analysis using a Quantachrome Autosorb-6 Pore Analyzer. Before the analysis, silica aerogels were degassed at 120 °C for 12 h and the adsorption–desorption isotherms were obtained at 77 K. Pore characteristics of the aerogels such as apparent surface area, total pore volume, micropore volume and average pore size of the samples were determined by using Brunauer–Emmett–Teller (BET), Barrett–Joyner–Halenda (BJH) and Dubinin-Radushkevich (DR) methods.

The morphology of the samples was examined via scanning electron microscopy (SEM) and Small-Angle X-ray Scattering (SAXS). SEM micrographs were obtained under 7.5 kV accelerating voltage in low vacuum mode at a magnification of 100,000 using a Thermo Scientific Apreo S instrument. SAXS measurements were carried out using a SAXSpoint 2.0 instrument (Anton Paar, Austria), operating with Cu Kα radiation and a hybrid photon-counting 2D EIGER R series detector over a Q-range of 0.08–5 nm^{-1}. Q is the momentum transfer defined as $Q = (2\pi/\lambda)sin\theta$, where λ is the used X-ray wavelength and θ is the half of the scattering angle.

The bulk density of the silica aerogels was determined from the mass-to-volume ratio obtained after drying, and the corresponding porosities were calculated according to Eq. (1):

$$\%Porosity = (1 - \rho_b/\rho_s) \times 100 \quad (1)$$

where ρ_s is the silica skeletal density, which is taken as 1.43 g/cm^3 for the organically functionalized silica backbone [39].

2.4. Antibiotic adsorption studies

Various batch experiments were performed in series to evaluate the adsorptive performance of the synthesized functional silica aerogels under different operating conditions. In a typical batch experiment for equilibrium isotherm studies, CIP solutions with various initial concentrations (5–125 mg/L) were mixed with 0.05 g adsorbent in a 50 ml erlenmeyer flask (m_{ads}/V_{soln} = 1 g/L), and the solution was shaken at 200 rpm on an orbital shaker for 24 h at atmospheric conditions and neutral pH (pH=6). The adsorbents were then separated from the solutions using a 0.22 μm syringe filter. The CIP concentration in the final solution was measured by UV–Vis Spectrophotometer (Shimadzu-UV 1800) at 273 nm. Each adsorption experiment was performed in triplicate to ensure the repeatability of the results. The effects of adsorbent dosage (m_{ads}/V_{soln} = 0.5, 1, 1.5) and solution pH (2,4,6,8,11) were investigated as operational parameters. During these experiments, the pH of the solutions was adjusted using either 0.2 M HCI or 0.5 M NH_4OH. The initial CIP concentration was set to 100 mg/L and the adsorption process was allowed to continue for 24 h.

Adsorption kinetic experiments were performed by changing the contact time of the adsorbate and adsorbent between 15–1440 min. Kinetic studies were carried out under ambient conditions at an initial CIP concentration of 100 mg/L, adsorbent dosage of m_{ads}/V_{soln} = 0.5 g/L, and solution pH of 6.

After every batch experiment, the equilibrium adsorption capacity ($q_e, mg/g$) and the removal efficiency ($RE, \%$) of the adsorbents were calculated according to Eq. (2) and Eq. (3), respectively:

$$q_e = \frac{(C_i - C_e) \times V_{soln}}{m_{ads}} \quad (2)$$

$$RE\% = \frac{(C_i - C_t)}{C_i} \times 100 \quad (3)$$

where C_i, C_t and C_e(mg/L) are the ciprofloxacin concentration at initial time, at any time t and at equilibrium, respectively. m_{ads} (mg) is the mass of the functional aerogel adsorbent and $V_{soln}(L)$ is the ciprofloxacin solution volume.

In equilibrium adsorption experiments which was conducted under ambient conditions at adsorbent dosage of 1, and solution pH of 6. the adsorption mechanism of the adsorbents was studied using the Langmuir and Freundlich equilibrium isotherm models. The linearized form of the model equation is given by Eqs. (4)–(5).

Langmuir isotherm model:

$$\frac{C_e}{q_e} = \frac{1}{q_m + K_L} + \frac{C_e}{q_m} \quad (4)$$

Freundlich isotherm model:

$$lnq_e = lnK_F + \frac{1}{n} lnC_e \quad (5)$$

In these equations, $q_m(mg/g)$ is the maximum adsorption capacity, $C_e(mg/L)$ is the equilibrium CIP concentration, $K_L(L/mg)$ is the Langmuir equilibrium constant, $K_F(mg/g)$ is the Freundlich equilibrium constant, and n is an emprical constant called heterogenity factor.

The adsorption kinetics of the aerogels were evaluated by fitting the experimental data to the pseudo-first-order, pseudo-second-order, intraparticle, and liquid film diffusion kinetic models (Eqs. (6)–(9)), respectively.

Pseudo-first order:

$$ln(q_e - q_t) = lnq_e - k_1 t \quad (6)$$

Pseudo-second order:

$$\frac{t}{q_t} = \frac{1}{k_2 q_e^2} + \frac{t}{q_e} \quad (7)$$

Intraparticle diffusion:

$$q_t = k_p t^{1/2} + C \quad (8)$$

Liquid-film diffusion:

$$\ln(1 - q_t/q_e) = -k_{fd} t \quad (9)$$

where q_t and q_e (mg/g) indicate the adsorption capacity at any time t and at equilibrium, respectively. $k_1(1/min), k_2(g/mgmin)$ and $k_p\left(mg/gmin^{-1/2}\right), k_{fd}(1/min)$ are the rate constants of pseudo-first order, pseudo-second order, intraparticle diffusion and liquid film diffusion models, respectively. C is a some model constant giving information about the thickness of the boundary layer. The values of the rate constants and model parameters were determined from the slopes and intercepts of the linearized plots of each model.

To assess the regeneration ability of the synthesized adsorbents, adsorption–desorption cyclic studies were carried out by utilizing different eluent solutions (0.5 M HCI and 0.5 M NH_4OH). The desorption experiments were performed by mixing 0.30 mg of CIP loaded adsorbent with 30 ml of eluent solution at a constant speed (200 rpm) under ambient conditions. After 240 min of contact, the suspension was centrifuged and the concentration of the supernatant was measured using a UV–Vis Spectrophotometer. After each desorption experiment, the functional adsorbents were washed with distilled water until pH=6

prior to the next cycle. The desorption capacity ($q_{e,des}(mg/g)$) of each cycle was determined by the equation below:

$$q_{e,des}(mg/g) = \frac{C_f \times V_{eluent}}{m_{CIP-load.ads}} \quad (10)$$

where V_{eluent}, $m_{CIP-load.ads}$ and C_f are the volume of the eluent solution, mass of the CIP loaded functional adsorbents and the final concentration (mg/L) of CIP measured in the eluent solution, respectively.

3. Results and discussion

3.1. Strucutral characterization of organofunctional silica aerogels adsorbents

Employing a wide array of structural characterization methods for organofunctional silica aerogel adsorbents is crucial for the design and optimization of adsorptive properties.

3.1.1. Chemical composition

3.1.1.1. FTIR spectroscopy. In Fig. 1, the characteristic bands originating from the different stretching vibrations of the silica backbone are prominent for all samples, exhibiting varying intensities. The band obtained at approximately 1040 cm^{-1} is related to the asymmetrical stretching vibration of the Si-O-Si bond, and according to the obtained intensities, the degree of silica polymerization is higher in S-VTMS than in S-GPTMS and S-TMSPM. Because of the steric hindrance of the large epoxide and methacrylate organic groups (Fig. S1) during silica polycondensation, S-GPTMS and S-TMSPM resulted in a lower degree of siloxane crosslinking, which was also confirmed by the NMR data. The other common band observed at 789 cm^{-1} is ascribed to the symmetric Si-O-Si stretching vibration and exhibits a change in intensity similar to the asymmetric stretching vibrations among the samples. The reference sample, S-BARE SILICA contains all the bands characteristic for siloxane stretching vibration confirming the well-developed silica network. In addition, a large shoulder near 1250 cm^{-1} appears, which is attributed to the longitudinal mode (LO) of Si-O-Si vibrations caused by Coulombic interactions [40]. For S-VTMS, S-GPTMS and S-BARE SILICA, the broad band centered at approximately 3400 cm^{-1} is related to the stretching vibrations of hydroxyl radicals in unreacted surface silanol groups [40]. The band observed near 950 cm^{-1} is also related to the stretching vibrations of surface silanols, and is visible only in S-TMSPM and S-BARE SILICA. Since the silsesquioxane network in S-BARE SILICA is free from any organic attachment, observed no C-related signal in this sample as expected and it exhibited more prominent –OH related signals at 950 cm^{-1} and near 3400 cm^{-1} as the surface of the silica is covered by the silanol polar groups. The distinct band appearing at approximately 1270 cm^{-1} is detectable only for S-VTMS and S-GPTMS and corresponds to the asymmetric deformation mode of the C–H bonds [41] originating from either the ethyl group of MTES or the vinyl/epoxide groups of functional silanes in the samples.

The successful functionalization of the silica surfaces was confirmed by the remaining bands in the spectra corresponding to vinyl, epoxide, and methacrylate radical groups.

S-VTMS exhibited several distinct bands characteristic of the vinyl moieties. The bands appearing at wavelengths of 967, 1410, 2983, and 3067 cm^{-1} were attributed to the wagging, scissoring, symmetrical, and asymmetrical vibration modes of the CH_2 group, respectively [41]. The signal at 1603 cm^{-1} resulted from the stretching vibrations of C=C in the vinyl group.

For S-GPTMS, the small peak observed near 690 cm^{-1} was attributed to the out-of-plane bending of the C-O-H group in epoxide [42]. The slight signals appearing as small shoulders at 850 cm^{-1} and 910 cm^{-1} are related to the asymmetric stretching of the epoxy ring, indicating that GPTMS did not undergo a ring-opening reaction owing to the mild synthesis conditions, and the ring structure was retained in the sample [43]. The peak observed at 1410 is to the in-plane bending vibration of the C-H bonds in the $-C(CH_3) = CH_2$ structure [44]. The band near 1460 cm^{-1} and two bands observed between 2800–3000 cm^{-1} are ascribed to the stretching vibration of the C-H bonds of the alkyl groups in the organic network [45].

In TMSPM TMSPM-derived sample, several emerging peaks were observed at wavelengths between 1300–1700 cm^{-1}. The bands at 1310 and 1325 are attributed to the stretching vibrations of the C-O-C bonds in the acrylate structure [45]. The slight bands near 1406 and 1467 cm^{-1} were due to the different stretching vibrations of the C-H bond of the alkyl groups of the organic substitution. The more prominent band at 1639 cm^{-1} and the distinct bands appearing as two shoulders at 1697 and 1718 cm^{-1} are ascribed to the stretching vibrations of C=C and C=O in the methyl methacrylate moieties in the silica structures, respectively [43,46].

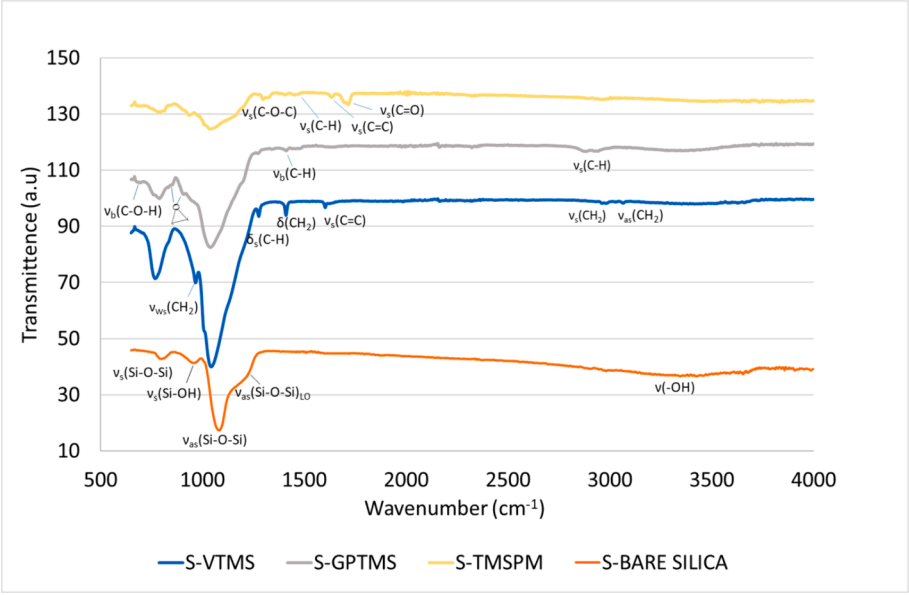

Fig. 1. FTIR spectra of silica aerogel adsorbents prepared from different organosilanes.

3.1.1.2. ^{29}Si-MAS-NMR spectra. The solid-state ^{29}Si MAS NMR spectra of the aerogels are presented in Fig. 2 to provide further information about the silicon environment and degree of organic functionalization on the silica surface. In $^{the\ 29}$Si MAS NMR spectra, Q^n and T^n notations are used to describe Si-based quaternary oxygen tetrahedra and three oxygen and one organic group tetrahedron, respectively, where n represents the number of siloxane groups bonded to the silicon atom. In Fig. 2, two main peaks indicating silica clusters comprising siloxane groups (Q^4) and some isolated silanol groups (Q^3) were observed at approximately − 110 ppm and − 101 ppm, respectively, in the Q^n region [30]. For S-VTMS, Q4 was the only dominant signal, proving a high degree of TEOS polycondensation and the successful formation of the siloxane network. The intensity of the Q^4 peaks of S-GPTMS and S-TMSPM was lower and was accompanied by Q^3 structures, confirming the presence of surface –OH groups resulting from the incomplete condensation of TEOS. The decreasing intensity of the Q^4 signals in these samples is attributed to the decrease in silica crosslinking during TEOS polymerization due to the steric restrictions imposed by the bulky organic chains of the selected functional silanes, which is in accordance with the FTIR results.

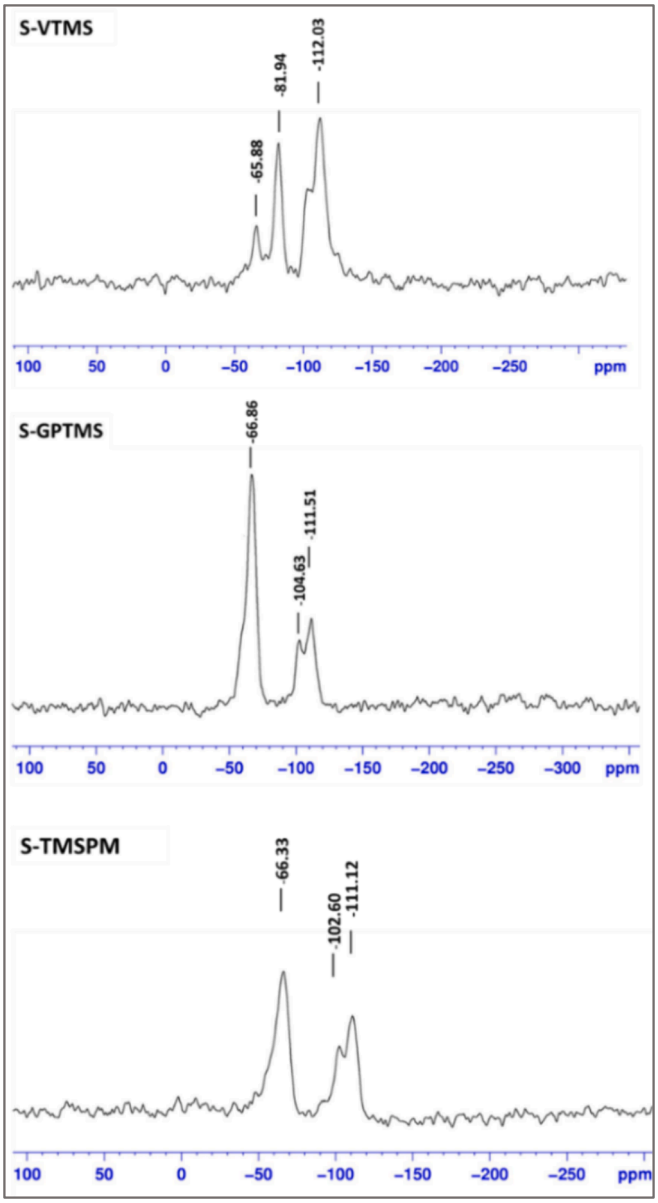

Fig. 2. 29Si-MAS-NMR Spectra of the organofunctional silica aerogels.

Along with the Q^n structures, T^n resonances were also apparent in the spectra because of the co-condensation of trialkoxysilanes with TEOS. The species detected on the silica surface in the form of T^3 signals near −66 ppm in S-GPTMS and S-TMSPM were assigned to the tri(T^3)-fold Si–O-linked silicon structures and refer to the complete condensation of trifunctional silanes and chemical attachment of the organic groups to the silica surface [47,48]. The same signal, however, shifted near − -82 ppm for S-VTMS, where the Si atom is directly bonded to the vinyl group, as reported in previous studies [49]. For vinyl-modified silica structures, the slight additional signal appearing at-65 ppm corresponds to T^1 resonance, which is ascribed to Si units with one siloxane bridge and two non-bonding oxygen groups. This additional peak shows that, even to a low extent, there are also some hydroxyl-rich sides on the silica surfaces of S-VTMS, which is also reflected in the FTIR findings.

For systems comprising silanes with long alkyl chains and polymerizable epoxide and methacrylate functional units, the final organic–inorganic hybrid structure is highly dependent on the condensation of inorganic components (siloxane units), as well as the existence and/or extent of polymerization in organic epoxide and methacrylate functional units. Therefore, for S-GPTMS and S-TMSPM, the incorporation of organic functionalities into the silica structure was further investigated by ^{13}C-CP-MAS NMR spectrophotometry, and the obtained spectra together with labeled carbon atoms in their molecular structure are depicted in Fig. 3.

Both in GPTMS and TMSPM-functionalized aerogels, the characteristic signals for the glycidoxypropyl and methacryloxypropyl groups were observed in the ^{13}C-CP-MAS NMR spectra. The glycidoxypropyl unit of GPTMS contains an epoxy ring, which under particular conditions is capable of forming various chemical species, such as diols, dioxane rings, terminal ethyl ether moieties, and polyethylene oxide chains (Fig. S3). Diols and methyl/ethyl ether groups can be formed depending on whether the opened epoxy ring reacts with acidic water or alcohols. Short polyethylene chains can also be formed in the structure through polyaddition reactions. According to Fig. 3, the signals appearing at approximately 7, 14, 16, and 22 ppm are ascribed to the first and second carbon atoms of GPTMS attached to the silicon atom [50]. The sharp peaks obtained near 49 and 42 ppm were due to the C5 and C6 carbon atoms in the epoxy ring, indicating that the GPTMS did not undergo complete ring-opening reactions during synthesis, which was also confirmed by the FTIR results [51]. On the other hand, the less intense peak observed at 58.28 ppm related to the terminal methyl/ethyl ether groups and the sharp peaks between 70–73 ppm related to the C atoms in poly(ethyleneoxide) chains show that hydrolytic ring-opening reactions and polymerization reactions of the opened epoxy ring have also taken place to some extent [52]. The additional slight signals that appeared in the 62–65 ppm region can be attributed to the methoxy groups bonded to the Si atom, which may come from either GPTMS or MTES during sol–gel reactions [51]. In the S-TMSPM, the intense peaks at 7.12 and 20.98 ppm are attributed to C1 and C2 carbon atoms in methylene groups attached to Si atom, respectively [50]. The peak obtained at 16.54 ppm is related to the C7 atom in the = C-CH_2 structure. The signals observed in between 44–58 ppm as well as the smaller signal obtained at 83.78 ppm correspond to C atoms in non-hydrolyzed methoxy groups (–OCH_3) retained in the structure [47,53]. The peak at 65.67 ppm was ascribed to the C3 atom belonging to the O-CH_2 unit in TMSPM [50]. The characteristic signals appearing near 123 and 135 ppm are attributed to the vinylic carbons (=CH_2 (C6) and = C-CH_3 (C5)) and the peaks near 166 and 175 ppm carbonyl carbons (C=O (C4)) in the methyl methacrylate organic group. In line with the FTIR results, they confirm the methacrylate functionality of the sample [48].

3.1.2. Morphological properties

3.1.2.1. SEM micrographs. SEM micrographs of the synthesized inorganic–organic hybrid adsorbents revealed various porous

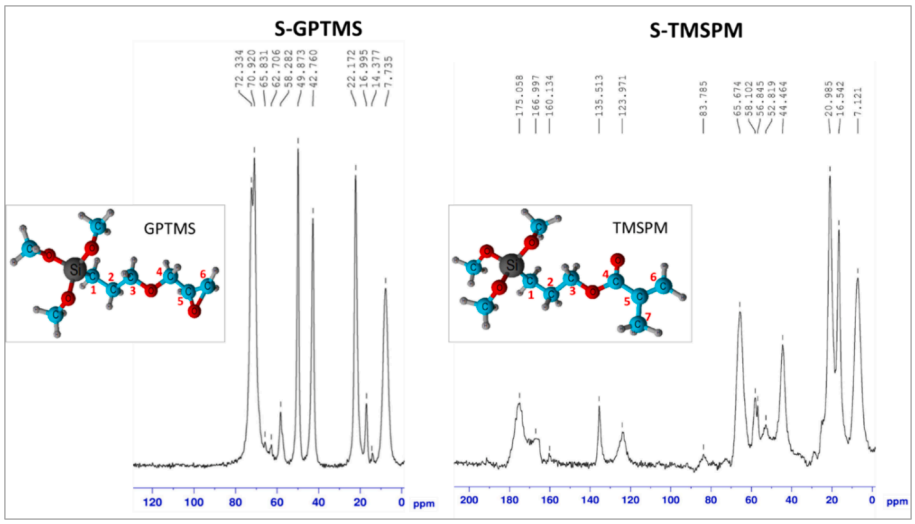

Fig. 3. 13C-CP-MAS NMR Spectrum of S-GPTMS and S-TMSPM.

microstructures in the size range of 1–200 μm. During the evolution of these hybrid structures, the hydrolysis and condensation reaction rates of the tri- and tetraalkoxysilanes played a crucial role in the formation of the porous morphology. Because of the faster reaction kinetics of tetraalkoxysilanes, primary particles with a SiO_2 core were generated as a result of TEOS condensation, initially forming smaller pores between these primary silica particles. The comparatively slower hydrolysis and condensation rates of trialkoxysilanes with vinyl, epoxide, and methyl functional groups resulted in condensation of these silanes onto the surface of the initially formed clusters, creating larger particles with

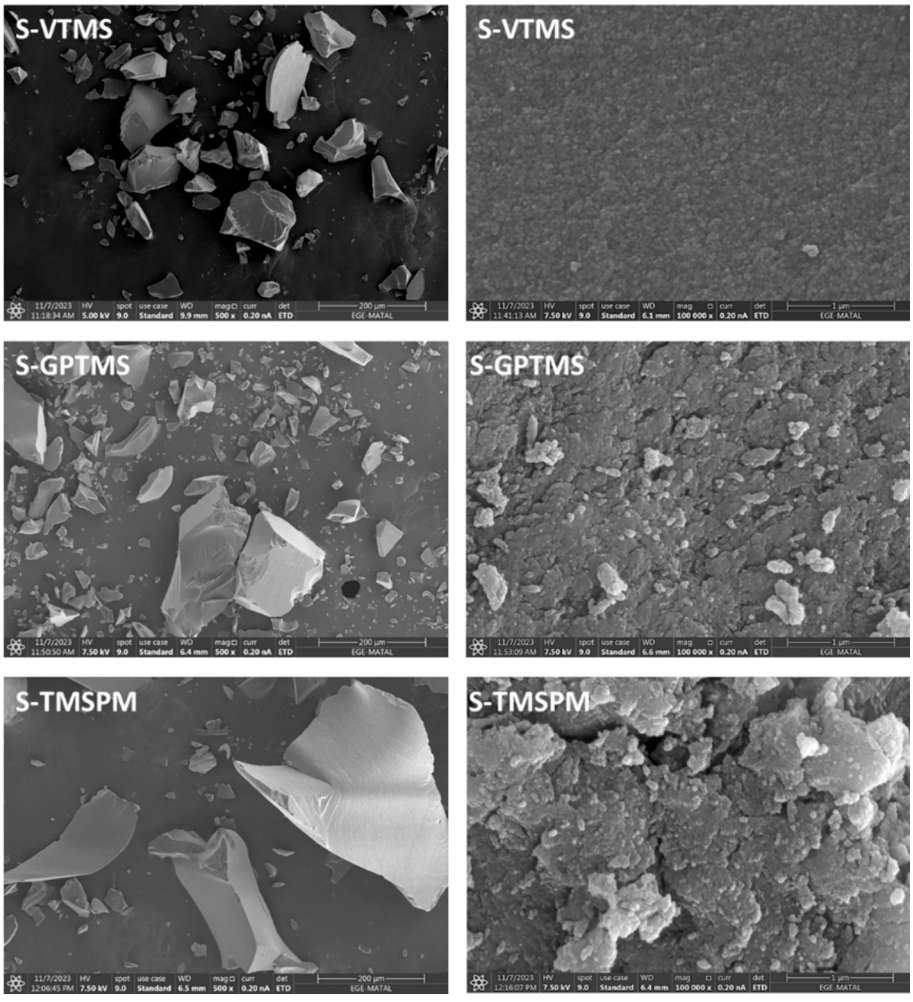

Fig. 4. SEM micrographs of the organofunctional silica aerogels under 500 and 100,000 magnification.

larger pores. Both the particle and pore sizes in the final network were strongly influenced by the attached organic groups on the silica surface. As shown in Fig. 4, the samples exhibited a network of particle aggregates rather than a typical chain-like morphology, which is typically obtained in solely TEOS/TMOS-derived systems. S-VTMS displayed a more uniform morphology comprising finer silica particles and smaller pores. In S-GPTMS and S-TMSPM, irregular growth of the secondary particles as agglomerated clusters was distinct, which triggered the formation of randomly distributed larger pores, resulting in a less compact morphology.

This is because bulky epoxide and methacrylate terminal groups cover the silica surface to a greater extent than the smaller vinyl and methyl radicals. This steric effect hindered the complete condensation of the surface silanol groups and lowered the degree of siloxane bridging in the network. S-TMSPM possessed a looser network with densely packed silica particles, as evidenced by the few micrometer-sized macropores and distinct accumulation of clusters in the SEM images. Moreover, the additional formations that appeared as microbeads with different contrasts in the SEM micrographs of all samples could be attributed to the small oligomers resulting from the self-condensation of excess trialkoxysilanes [52].

3.1.2.2. SAXS profiles. The morphological properties of the synthesized aerogels were further examined via SAXS analysis, and the SAXS scattering curves of the adsorbents are depicted in Fig. 5.

The SAXS curves of the S-VTMS sample exhibit characteristics typical of mesoporous materials [29,54]. The particle size of S-VTMS was estimated to be approximately 25*nm*. Because of the undefined, irregular shape of the particles, as observed in the SEM images, and their high polydispersity, model fitting was performed using a shape-independent one-level function. This function combines the exponential Guinier-type scattering at low Q with a power law scattering at high Q [55]. The diameters (D) were calculated from the gyration radius (Rg), assuming a spherical particle shape: $D = 2\sqrt{5/3}Rg$.

The vinyl functionalizing group occupied some of the available binding spaces, resulting in a nearly 20% reduction in the average particle size compared to that of the bare silica aerogel (Fig. S4). The power exponent for S-VTMS exhibited a value of 2.3, characteristic of volume or mass fractal systems, indicating that the nanoscale structure is a complex self-organized system. In this system, the particles contribute to space filling in a fractal-like manner.

The structures of the S-TMSPM and S-GPTMS samples, as confirmed by SEM measurements, exhibited larger particle sizes. Consequently, only the surface characteristics can be analyzed within the size range studied by SAXS. The scattering curves were fitted with two power-law functions, and the crossover values of these two functions were determined.

The crossover in Q corresponds to a characteristic size value calculated as $2\pi/Q$, which delineates a rough boundary between two size ranges for which the scattering intensities can be characterized by power laws. The complexity of the studied system suggests that the high-Q range, corresponding to smaller sizes, would exhibit fractal-like behaviour with fractal dimensions between 2 and 3. This indicates that the structures are highly ramified, branched, or porous. It can be inferred that the small primary particles are composed of highly ramified branching molecular structures.

Table 1
SAXS results of S-GPTMS and S-TMSPM.

Sample	Small-Q power	High-Q power
S-TMSPM	3.96 ± 0.06	1.32 ± 0.02
S-GPTMS	4.29 ± 0.04	1.71 ± 0.05
Cross-over ($2\pi/Q$)	approx. 42 nm	approx. 32 nm

The low-Q range, corresponding to larger sizes in real space, suggests that the size of the particles, composed of the primary particles seen in the high- Q range, exceeds the range covered in the present experiment, that is, the particles are larger than several tenths of nanometers. The surfaces of these particles in the case of the S-TMSPM sample appear smooth (with $p = 4$ indicating smooth surfaces), while in the case of the S-GPTMS sample, there is a density gradient ($p > 4$) at the interface between the particles and pores (Table 1).

3.1.3. Textural properties

3.1.3.1. N_2 sorption. The textural properties of the aerogels obtained from the N_2 sorption and bulk density measurements are summarized in Table 2. The low bulk density (<0.173 g/cm^3) and very high porosity (>92 %) proved that all samples were obtained in a lightweight form. Nevertheless, the differences in the attached organic groups on the silica surface led to significant alterations in the porous structures of the samples. The previously presented SEM and SAXS results showed that the sizes of the secondary particles and pores comprising the silica network in S-VTMS were much smaller than those of S-GPTMS and S-TMSPM, which predominantly fall in the mesoporous range. In line with these observations, the N_2 sorption results also confirmed the mesoporous morphology of S-VTMS, with a high apparent surface area (892 m^2/g) and total pore volume values (1.02 cm^3/g). As depicted in Fig. S5, the type IV isotherm of S-VTMS was accompanied by a hysteresis loop of type H3, which is specific to materials with plate-like particles with wedge-shaped/grooved pores. The H3 type of hysteresis loop is also characterized by the existence of some macropores, which are not completely filled by the pore condensate. The macropore domain was even more evident in S-GPTMS and S-TMSPM. Since only the pore sizes up to 50 nm are detectable in N_2 sorption analysis, BET measurements remained insufficient for the precise determination of macro and mesopore distribution within the samples S-GPTMS and S-TMSPM. Despite being highly porous, the low mesopore volume and apparent surface area values obtained from the porosimetry measurements were ascribed to the deformable macropore domains of these samples. For such materials, compression of loose macropores during N_2 intrusion is the main reason for the underestimation of the obtained surface area, total pore

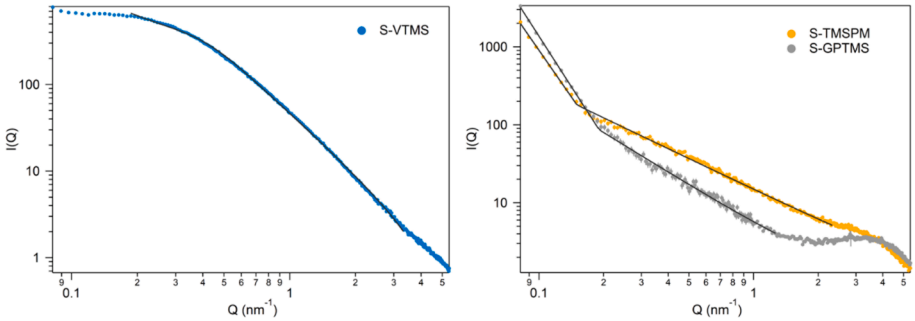

Fig. 5. SAXS curves of the adsorbents.

Table 2
Pore properties of the synthesized organofunctional silica aerogels.

Pore Properties	Sample ID		
	S-VTMS	**S-GPTMS**	**S-TMSPM**
Apparent Surface Area (m^2/g)	892	9.4	19.4
DR Micro Pore area (m^2/g)	54	4.86	13.1
Total Pore Volume (cm^3/g)	1.02	0.0094	0.026
DR Micro Pore volume (cm^3/g)	0.32	0.0017	0.0046
BJH Avarage Pore Diameter (nm)	4.32	1.88	2.13
Bulk Density (g/cm^3)	0.094	0.173	0.156
Porosity (%)	96	92	93

volume, and average pore diameter [39]. Table 2 also shows that all the samples contained a significant number of micropores. More than half of the pores detected in the 0–50 nm region belonged to micropores for S-GPTMS and S-TMSPM, whereas for VTMS, micropores occupied only 6 % of the total porous domain in the network.

3.2. Batch adsorption experiments

The adsorptive behaviors of the three functional aerogels and a reference aerogel for the removal of CIP from water were investigated via batch-wise experiments. The initial CIP concentration, adsorbent dosage, solution pH, and contact time were tested as operational parameters to determine the optimum working conditions for achieving the highest sorption capacity for specific adsorbents.

The relationship between the initial concentration and the adsorption capacity was revealed by contacting a fixed amount of aerogel adsorbents with varying concentrations of CIP solution for 24 h at a constant ambient temperature, and the results are depicted in Fig. 6. As the driving force for the mass transfer of CIP molecules increased with increasing initial CIP concentration, the obtained sorption capacity gradually increased up to 100 mg/L and then leveled off after 100 mg/L because of the saturation of the adsorbents for CIP uptake. The equilibrium adsorption capacities at the maximum CIP uptake were recorded as 50.32, 20.72, 42.03 and 46.77 mg/g for S-VTMS, S-GPTMS, S-TMSPM and S-BARE SILICA, respectively. In contrast, the highest RE (up to 90 %) was reached in the dilute CIP solution and tended to decrease as the CIP concentration in the water increased. The variations in the obtained maximum capacities can be attributed to the differences in the microstructural and surface characteristics of the samples, which will be discussed in detail in later sections.

The equilibrium data for the adsorbents were further evaluated using adsorption isotherms. The Langmuir and Freundlich models were used to analyze the adsorption isotherms of the samples (Fig. 7). For all samples, the Langmuir model fitted the experimental data best, with R^2 values varying between 0.977–0.994 verifying that adsorption is assumed to be monolayered, and each adsorbent contains homogenously distributed active sites with uniform binding energies [26]. The q_m values calculated using the Langmuir model, which is an important parameter for designing efficient adsorption systems for target pollutants, were also very close to the experimentally obtained equilibrium capacity values for each aerogel adsorbent (Table 3). The maximum capacities obtained in this study are also comparable to those of silica-based materials synthesized for the same purpose in the literature (Table 4).

The effect of different adsorbent dosages on the equilibrium capacity of the functional silica aerogels was also tested, as shown in Fig. 8. Regardless of the type of adsorbent, the equilibrium capacity recorded after 24 h of contact decreased with increasing adsorbent input, and the highest capacity (48–66 mg/g) was obtained at the lowest adsorbent dosage ($m_{ads}/V_{soln} = 0.5$). This was presumably due to the particle aggregation of the aerogels at high dosages, which limited the availability of the active sorption sites for CIP molecules.

The CIP adsorption capacity of the samples was evaluated as a function of time to determine the kinetic behavior of the synthesized adsorbents. As depicted in Fig. 9, in the first 30 min, the adsorption capacity increased almost linearly because of the vacancy of the active sides and the strong affinity between the adsorbent binding sides and adsorbate molecules. Except for S-GPTMS, all samples reached more than 70 % of their maximum capacity within 30 min and 60 min of contact, and the maximum adsorption capacity was reached for all samples, confirming fast sorption kinetics. The adsorption trends of the four aerogels over time were quite similar yet they ended up with different equilibrium capacities. This difference in the obtained capacities can easily be attributed to aerogels' differentiation in morphological and surface characteristics depending on attached functional groups on silica surface. Although in theory, adsorbents with high surface areas and high pore volumes are regarded as more efficient in uptake of large amounts of contaminants, it is shown in this study that the predominantly macroporous adsorbents S-TMSPM and S-GPTMS with low apparent surface area values of 19 m^2/g and 9 m^2/g also exhibited competitive sorption performances compared to S-BARE SILICA, which has the highest surface area (912 m^2/g) value among the series. Moreover, despite having similar textural properties and almost the same apparent surface area values, S-VTMS yielded better adsorptive performance for CIP molecules than unmodified silica aerogel. This observation clarifies that pore filling is not the only controlling mechanism of CIP adsorption, and molecular interactions between the organically functionalized surface of the silica and antibiotic molecules are equally important in determining the ultimate capacity of these adsorbents. After 60 min, noticeable changes in the adsorption capacities were only detectable for the S-VTMS and S-BARE SILICA. They showed a slight increase (5.6 % for S-VTMS and 7.6 % for S-BARE SILICA) in their adsorption capacity between 1 h and 24 h of contact duration, which can be attributed to the slow diffusion of CIP into the micropores of these aerogels. After 90 min, no noticeable changes were observed in the obtained capacity, indicating that the equilibrium time was 90 min for all samples.

To elucidate the underlying adsorption mechanism, the adsorption

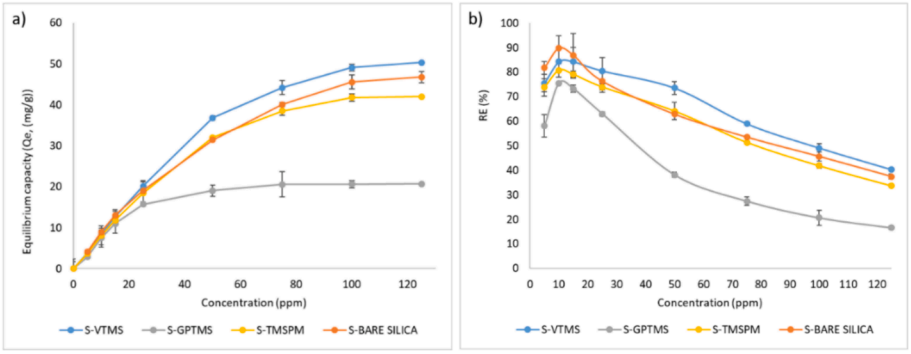

Fig. 6. Effect of initial CIP concentration on equilibrium capacity (a) and removal efficiency (b) of vinyl, epoxide and methacrylate functionalized silica adsorbents.

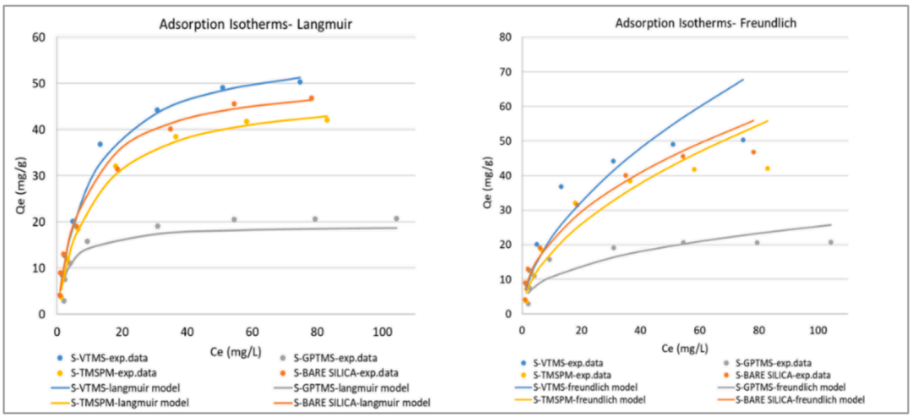

Fig. 7. Langmuir and Freundlich equilibrium adsorption isotherms of CIP on vinyl, epoxide and methacrylate functionalized silica aerogel adsorbents.

Table 3
Adsorption isotherm parameters.

Sample ID	$q_{e,exp}(mg/g)$	Isotherm Models					
		Langmuir Parameters			Freundlich Parameters		
		$q_m(mg/g)$	$K_L(L/mg)$	R^2	n	$K_F(mg/g)$	R^2
S-VTMS	50.33	58.47	0.095	0.987	1.803	6.192	0.883
S-GPTMS	20.72	19.26	0.297	0.977	2.701	4.617	0.722
S-TMSPM	42.03	48.54	0.092	0.994	1.869	5.243	0.907
S-BARE SILICA	46.77	51.54	0.116	0.992	2.134	7.253	0.916

Table 4
Comparison of maximum fluoroquinolone antibiotics adsorption capacities of silica-based adsorbents in literature.

Adsorbent Specification	Maximum Capacity (mg/g)	Ref.
Silica xerogels from volcanic tuff	24.5	[56]
Silica nanoparticles from rice husk	30.0	[16]
Protein modified nanosilica	85.0	[19]
ZnO supported SBA-15	32.3	[57]
Nanosilica form rice husk	74.1	[21]
Mesoporous silica nanoparticles	47.2	[27]
Diamine modified MCM-41	110	[28]
Mesoporous silica	15.0	[58]
Vinyl modified aerogel	66.1	This study

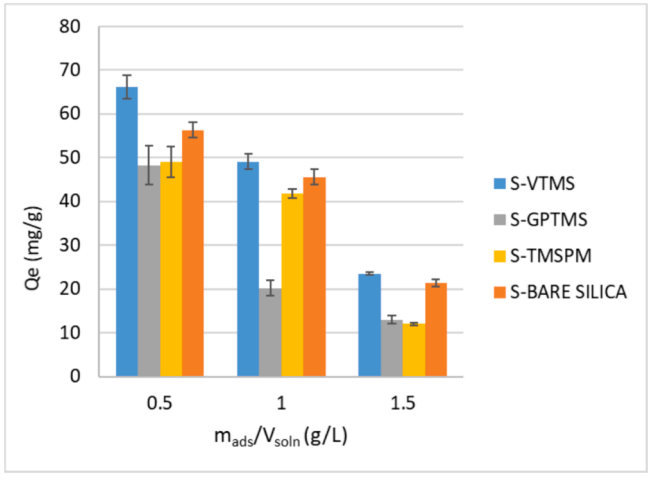

Fig. 8. Effect of adsorbent dosage on CIP adsorption capacity of silica aerogels.

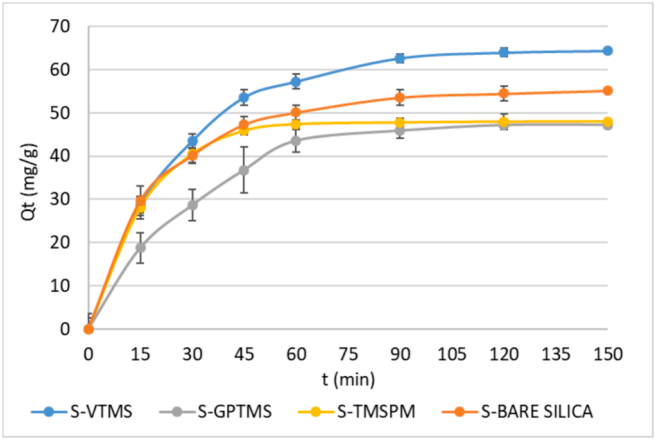

Fig. 9. Effect of contact time on the CIP adsorption capacity of silica aerogels.

kinetics were analyzed using different kinetic models. The model parameters and correlation coefficient values (R^2) obtained for each model are presented in Figs. 10, 11, and 5. For all the samples, the adsorption behavior was better described by a pseudo-second-order kinetic model ($R^2 > 0.97$), which means that the adsorption process was promoted by chemical attraction in dynamics with the assistance of physisorption. In particular, for S-TMSPM and S-BARE SILICA, the experimental Q_e values were in excellent agreement with the values calculated from the PSO kinetic model. For S-VTMS and S-GLYMO, the Qe values calculated by the PSO model were also quite consistent with the experimentally obtained equilibrium capacities (Table 5). Intraparticle and liquid film diffusion models were also applied to gain more insight into the diffusion mechanisms during the sorption process and the rate-limiting steps affecting the adsorption kinetics. As shown in Fig. 11, the plot of q_t vs. $t^{1/2}$ displayed multilinearity, and the lines did not pass through the origin, indicating that intraparticle diffusion is not the sole rate-limiting step, and the rate of adsorption is also controlled by external diffusion processes. In Fig. 11, the first linear part of the plot obtained for all samples

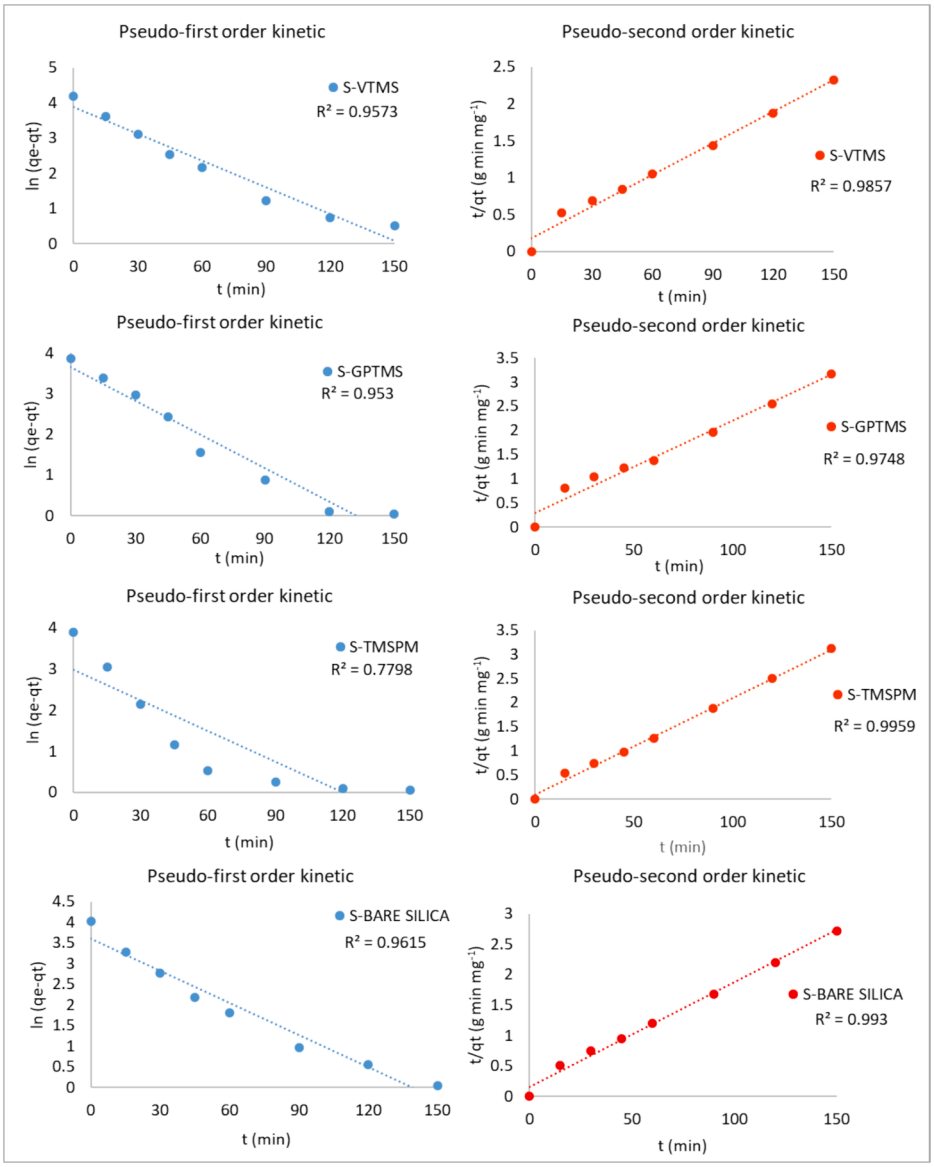

Fig. 10. Modelling of adsorption kinetics: Fitting of time-dependent CIP adsorption data on pseudo-first and pseudo-second models.

is about the external diffusion of the CIP molecules to the outer surface of the meso/macropores of the aerogels, which is driven by the concentration difference between the CIP solution and the outer surface of the aerogels, implying a fast adsorption process. The steepness of this line and the large intercept values in Fig. 11 indicate the domination of external diffusion over intraparticle diffusion; therefore, it could be regarded as the major rate-controlling factor in the adsorption kinetics of the synthesized aerogels. The second linear part, which is only distinguishable for S-VTMS and S-BARE SILICA, is ascribed to the internal diffusion through the inner micropores, confirming the open porous interconnected network of the samples with accessible active inner sides. The last section of the line is related to the equilibrium state of the adsorption. Having higher R^2 values in liquid-film diffusion model than in intraparticle diffusion model also suggest that film diffusion through the boundary liquid layer covering the external surface of the aerogels is the main rate-limiting step of CIP adsorption with the contribution of intraparticle diffusion. As a main consequence of this observation, higher adsorption capacities were obtained at high initial CIP concentrations because higher initial concentrations of CIP solution led to the generation of a higher gradient for the diffusional mass transfer of CIP through the boundary layer around the aerogels. In brief, the kinetic models for the functionalized silica aerogel adsorbents in this study confirm that the adsorption process is mainly governed by chemical attractions and that the adsorption rate is controlled by external diffusion with the contribution of intraparticle diffusion.

Since CIP is a special molecule that can possess different charge states under different acid-base conditions, the effect of solution pH on CIP adsorption on functional silica aerogels was also investigated, and the results are shown in Fig. 12. Resulting from having two acid dissociation constants (pK_{a1} = 6.1 and pK_{a2} = 8.7), CIP exists in three different ionic forms depending on the pH of the media [26,59]. Because of the protonation of the amine moieties in its structure, CIP molecules are in the cationic form when the solution pH is < 6.1. Above pH=8.7, the anionic CIP species became dominant in the solution because of the deprotonation of the carboxylic group. At a solution pH between 6.1——8.7, CIP molecules were in the zwitterionic state because of the simultaneous presence of negatively charged carboxylate moieties ($–COO^-$) and positively charged amine moieties ($–NH_3^+$) in the aqueous solution. To unveil the impact of electrostatic interactions on the adsorptive performance of the adsorbents, the surface charge characteristics of the functional aerogels and bare silica aerogels were investigated using point of zero charge (pzc) measurements (Fig. S6). After

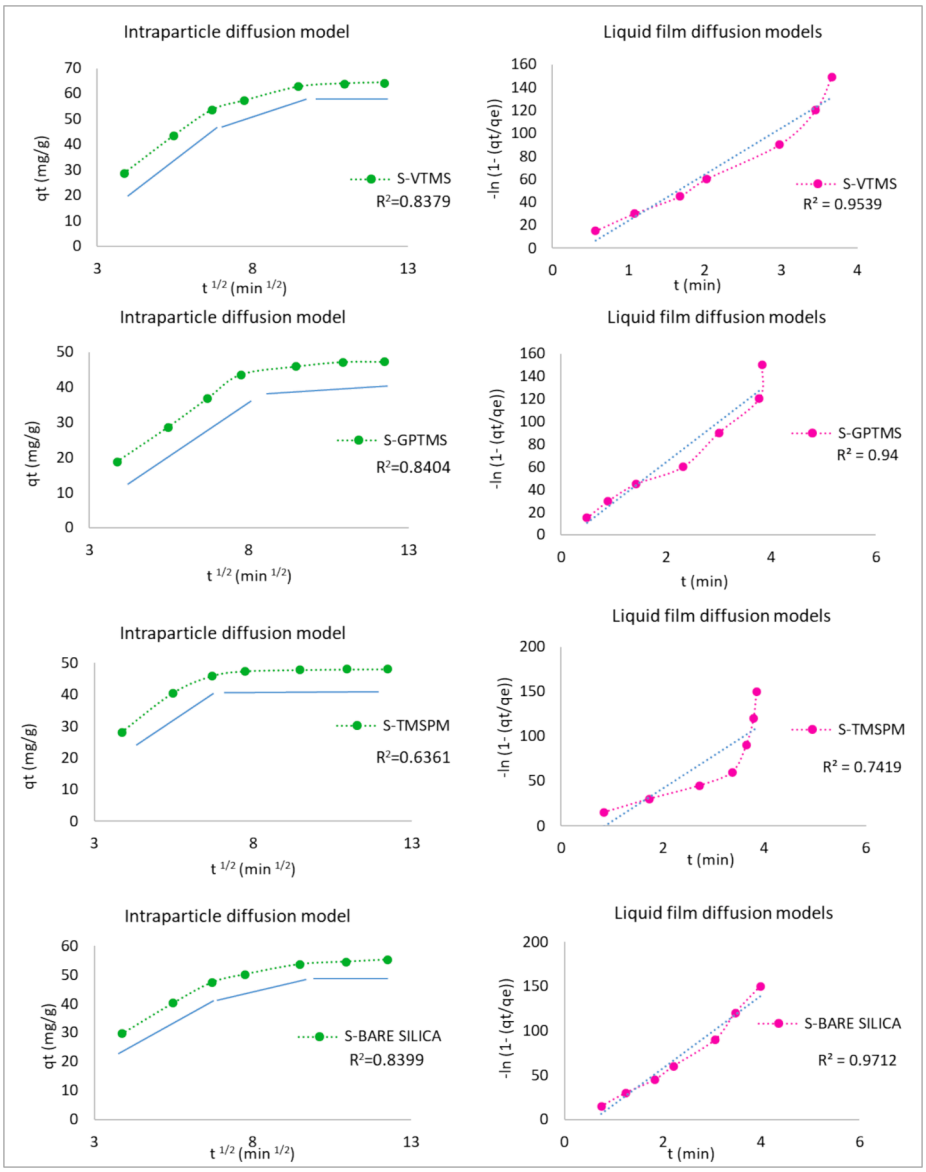

Fig. 11. Modelling of adsorption kinetics: fitting of the time-dependent CIP adsorption data to the intraparticle and liquid diffusion kinetic models.

Table 5
Kinetic model parameters for CIP adsorption.

	$Q_{e,exp}$	Pseudo-first order			Pseudo-second order		
		$k_1(1/min)$	$Q_{e,calc}(mg/g)$	R^2	$k_2(g/mgmin)$	$Q_{e,calc}(mg/g)$	R^2
S-VTMS	66.08	0.0247	42.98	0.9148	0.0011	69.93	0.9857
S-GPTMS	48.26	0.0276	39.26	0.9335	0.0012	55.63	0.9748
S-TMSPM	49.08	0.0244	19.97	0.7806	0.0039	50.00	0.9959
S-BARE SILICA	56.24	0.0252	34.01	0.9615	0.0019	58.13	0.9930

the experiments, the pzc values of S-BARE SILICA, S-VTMS, S-GPTMS, and S-TMSPM were determined to be 2.2, 3.5, 4, and 3.2, respectively, indicating that the surface of the adsorbents was positively charged at pH values lower than the pzc of the corresponding adsorbent and vice versa. Therefore, owing to the strong repulsion between the positively charged surface groups of CIP molecules and the functionalized aerogels, the adsorption process was significantly obstructed under strongly acidic conditions (pH=2). Between pH=4–6, the surfaces of all adsorbents were negatively charged and CIP molecules were still in cationic form, so that the obtained sorption capacity significantly increased and reached its maximum at pH=6 owing to the enhanced electrostatic attraction. After pH=6, because CIP molecules were in their neutral form, strong electrostatic attractions lost their dominance and the sorption capacity started to decrease. Nevertheless, an obvious increase in the sorption capacity was observed after pH=8 for S-GPTMS and S-TMSPM, which could be indicative of additional mechanisms besides electrostatic interactions in the determination of final sorption capacities. In strong alkaline conditions (pH>10) as reported in previous studies, epoxy group retained in the silica structure transforms into diol groups by further ring opening reactions [60]. The possible increment in the number of diol groups attached to the silica improved the adsorption ability of S-GPTMS on CIP as a results of enhanced π-π EDA and

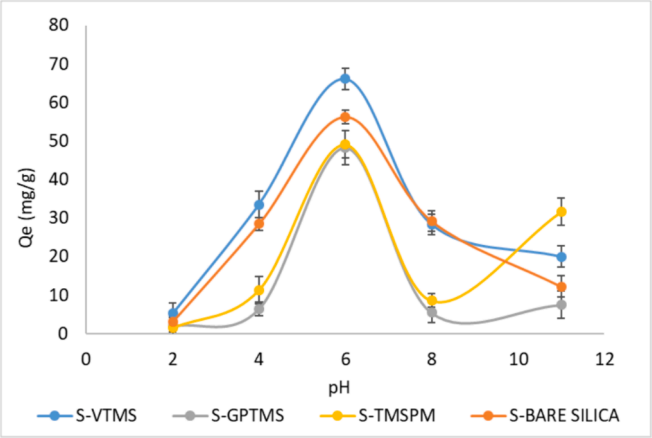

Fig. 12. Effect of solution pH on the CIP adsorption capacity of silica aerogels.

hydrogen bonding interaction. Despite the diminishing of electrostatic attraction, the increment on the adsorptive capacity of S-TMSPM could be attributed to the domination of other contributing mechanisms to the overall adsorption process.

As can be deduced from the previous discussions, physical interactions, such as pore filling or electrostatic interactions, might not be the only mechanism affecting CIP adsorption on the functional aerogel adsorbents in this study (Fig. 13). In particular, for S-GPTMS and S-TMSPM, rather than pore filling, chemical interactions such as π-π electron-acceptor–donor (EDA) interactions and hydrogen bonding seemed to play a dominant role in facilitating the adsorption of CIP onto these adsorbents. Due to presence of a fluorine group with strong electronegativity in its molecular structure (Fig. S1), CIP molecule can act as a π-electron acceptor [61]. On the other hand, the hydroxyl groups on the silica surface behave as π-electron donors. Alkyl radicals attached to the carbon atoms in the modified silica surfaces also behave as electron donors, resulting from both inductive and hyperconjugation effects, whereas vinyl, epoxide, and methacrylate functional moieties on silica aerogels usually play dual roles as both electron acceptors and donor [62,63]. Therefore, π-π EDA interactions could be an important factor promoting the adsorption of CIP in both samples. In addition to π-π EDA interactions, CIP containing –NH–, –COOH, –C=O, and –F functional groups also tended to form hydrogen bonds with the oxygen-containing functional groups of S-GPTMS and S-TMSPM, which was also reflected in the FTIR spectra (Fig. 14) obtained after CIP adsorption [64].

In the FTIR spectra obtained after CIP adsorption, the samples were characterized by new emerging peaks, confirming the presence of CIP molecules stored in the pore channels or on the surface of the functional silica aerogels (Fig. 14). The band observed near 830 cm^{-1}, which was only distinguishable for S-VTMS and S-GPTMS, was attributed to the out-of-plane deformation modes of the C-H bond in aromatic mono/polycyclic rings in the CIP molecule [65]. The intensity of the peak at approximately 1270 cm^{-1} increased in all samples with CIP loading and was ascribed to the conjugation of the stretching vibrational C-O band and bending vibrational –OH band in the carboxylic acid structure of CIP [66]. The signals obtained in the spectral region between 1400 and 1465 cm^{-1} are related to the stretching vibrations of the C-O bonds in the carbonyl groups of CIP, and they are more obvious in S-TMSPM than in S-VTMS and S-GPTMS. The common signals that appeared at 1630 and 1728 cm^{-1} are attributed to the N-H bending vibration in the quinolone structure and the C=O stretching vibration of the carboxylic acid group in CIP molecules, respectively [67]. Although they appeared in S-VTMS and S-GPTMS as small shoulders, their intensity was much higher in S-TMSPM, confirming the abundance of adsorbed CIP in this sample. The –OH-related signals appeared as large bands at approximately 3500 cm^{-1}, which became more obvious after CIP loading. With the CIP loading the –OH- related vibrations displayed slight shifting in all samples (Fig. S7). The changes in both in the intensity and the position of these bands could be ascribed to the formation of hydrogen bonds between the carboxyl and/or hydroxyl groups of the CIP molecules and the surface silanol or oxygen-containing functional groups of the adsorbents. At the same time, it could also be attributed to the –OH groups in carboxylic group in the CIP structure.

3.2.1. *Regeneration studies*

For practical applications, the regeneration and reusability of the adsorbents were investigated using cyclic tests. Since the weaker adsorption interaction between the adsorbent and adsorbate indicates an easy desorption process, and the pH is a crucial factor in determining the extent of dissociation of the adsorbed molecules from the surface of the adsorbent, both acidic (0.5 M HCI) and basic (0.5 M NH_4OH) solutions were used as eluents to remove the adsorbed CIP molecules from the functional aerogels. The obtained results were presented in the Fig. 15. The desorption tests were repeated until the samples preserved over 80 % of their initial capacity. At the initial stage, the desorption efficiency correlated positively with time; more than 85 % of CIP was desorbed within 60 min for all samples, and the obtained efficiency

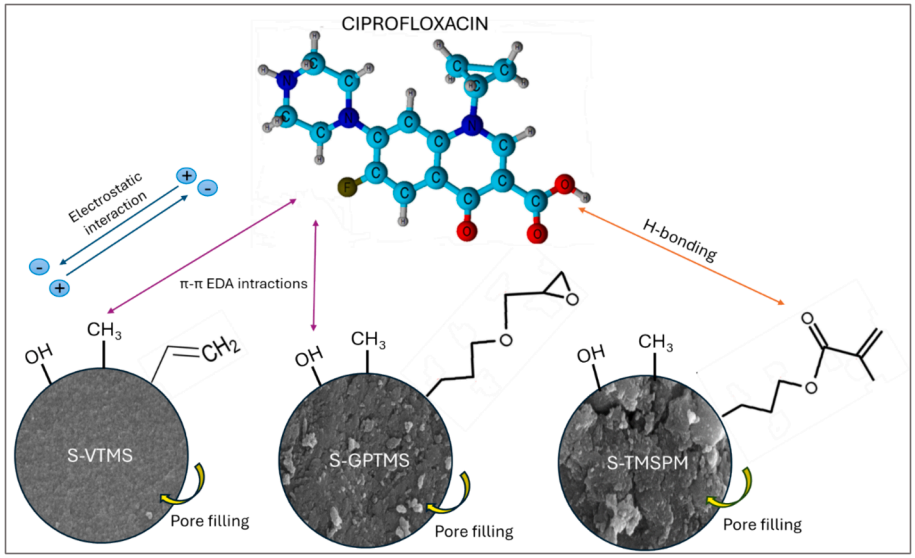

Fig. 13. Schematic representation of CIP adsorption mechanisms on functionalized silica aerogel adsorbents.

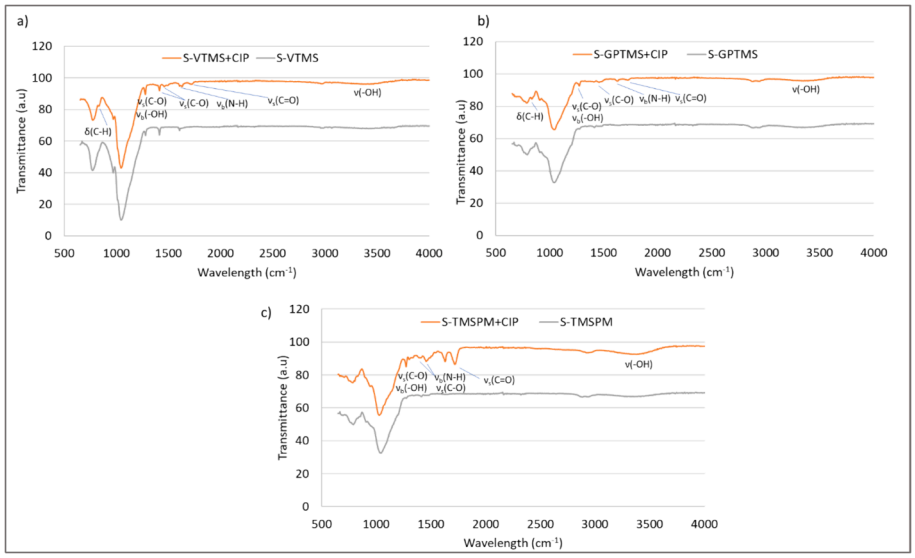

Fig. 14. FTIR spectra of the silica aerogels after CIP adsorption a) vinyl-modified silica aerogel, b) epoxy-modified silica aerogel and c) methacrylate-modified silica aerogel.

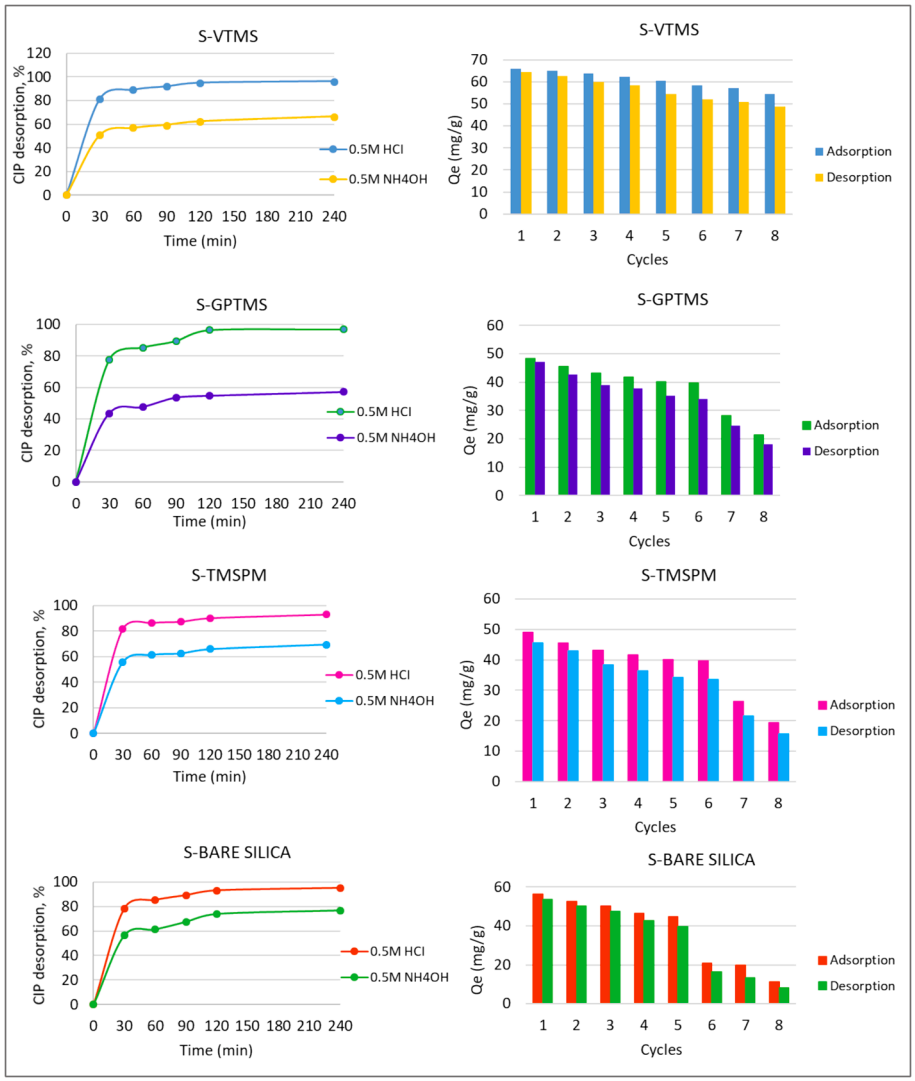

Fig. 15. CIP desorption efficiency in different effluents and regeneration cycles of the functionalized aerogels.

stabilized after 120 min. As previously mentioned, under strong acidic conditions, due to the protonation of CIP ((R_2-N-H_2^+)), antibiotic molecules hardly adsorbed on the positively charged adsorbent surfaces, which made CIP desorption very easy. Similarly, under strongly basic conditions, due to the deprotonation of the carboxylic group in CIP, the adsorbent and adsorbate molecules were in anionic form, which also hampered electrostatic attraction. Nevertheless, the obtained adsorption capacity was still higher than that under strongly acidic conditions (Fig. 12). In parallel with the weaker adsorptive interactions, strongly acidic conditions easened the dissociation of the adsorbed molecules during the desorption process better than under strongly basic conditions. With an acidic eluent, the maximum desorption efficiencies calculated after 24 h of exposure were 97.6 %, 97.5 %, 93.1 %, and 95.1 % for S-VINYL, S-GPTMS, S-TMSPM, and S-BARE SILICA, respectively. S-TMSPM, which had the lowest desorption efficiency compared to the other samples, could also be another indication of stronger molecular interactions between the methacrylate functional silica surface and CIP molecules.

Without a significant loss in their adsorptive capacity, S-VTMS retained its adsorptive performance for up to eight cycles, whereas S-GPTMS and S-TMSPM exhibited durable cyclic performance over six cycles, and S-BARE SILICA had repeatable sorption ability up to five cycles. The change in the decreasing adsorption capacities for each sample could be attributed to the partial deterioration of the active binding sites of the adsorbents, as well as the presence of residual CIP molecules retained in the structure. Nevertheless, durable sorption performance over several cycles is a good sign for the efficient use of functional silica adsorbents in antibiotic removal applications from environmental and economic points of view.

4. Conclusion

In this study, organofunctional silica aerogel adsorbents were synthesized via a one-pot sol–gel method under ambient conditions to remove ciprofloxacin molecules from water. Various organofunctional silanes with vinyl, epoxide, and methacrylate functional groups were incorporated into sol–gel reactions as silica co-precursors to modify the gel surface. NMR and FTIR results proved successful network formation with effective surface functionalization. The SEM images displayed particle-aggregated clustered structures for all samples. The differences in the incorporated organic groups significantly altered the network compactness by changing the size of the pores and particles in the network. S-VTMS exhibited a more compact morphology with finer secondary particles and smaller pores, whereas S-GPTMS and S-TMSPM were characterized by larger pores and agglomerated large silica particles, as indicated by SAXS analysis. The N_2 sorption results also confirmed the mesoporous morphology of S-VTMS, whereas in S-GPTMS and S-TMSPM, there were obvious macropore domains in the network. The prepared aerogels were then evaluated as ciprofloxacin adsorbents via batch sorption experiments and under the optimum operating conditions (C_0 = 100 mg/L, m/V=0.5, pH=6, t = 90 min) the equilibrium capacities were 62.7, 45.8 and 47.8 mg/g for S-VTMS, S-GPTMS and S-TMSPM, respectively. Equilibrium and kinetic studies revealed that the adsorption of ciprofloxacin molecules best fitted the Langmuir isotherm model and pseudo-second-order kinetic model for all the samples. These results showed that the adsorption process was promoted by the chemical attraction between the attached functional groups on the silica surface and ciprofloxacin molecules with the assistance of physisorption. Therefore, despite having a low surface area, both S-GPTMS and S-TMSPM had similar maximum capacities as S-VTMS. The regeneration studies confirmed that the synthesized adsorbents were suitable for repeatable usage over several cycles (eight for S-VTMS, six for S-GPTMS, and S-TMSPM). Overall, the highly competitive sorption capacity, fast sorption kinetics, and reusability make these aerogels excellent candidates for application as efficient adsorbents for antibiotic removal from aqueous media in the future.

Declaration of competing interest

The authors declare that they have no known competing financial interests or personal relationships that could have appeared to influence the work reported in this paper.

Data availability

Data will be made available on request.

Acknowledgement

This study was financially supported by the Ege University Office of Scientific Research Projects under Contract Number 23943. Authors thank the help of Manfred Kriechbaum for his assistance in the X-ray measurements. The authors acknowledge the CERIC-ERIC Consortium for the access to experimental SANS&SAXS facilities and financial support (Proposal ID 20232184). The authors would like to acknowledge the use of the Somapp Lab, a core facility supported by the Austrian Federal Ministry of Education, Science and Research, the Graz University of Technology, the University of Graz, and Anton Paar GmbH.

Appendix A. Supplementary data

Supplementary data to this article can be found online at https://doi.org/10.1016/j.seppur.2024.129112.

References

[1] T.M. Darweesh, M.J. Ahmed, Adsorption of ciprofloxacin and norfloxacin from aqueous solution onto granular activated carbon in fixed bed column, Ecotoxicol. Environ. Saf. 138 (2017) 139–145, https://doi.org/10.1016/j.ecoenv.2016.12.032.

[2] A. Mohseni-Bandpei, A. Eslami, H. Kazemian, M. Zarrabi, S. Venkataraman, M. Sadani, Enhanced adsorption and recyclability of surface modified hydrophobic silica aerogel with triethoxysilane: removal of cefixime by batch and column mode techniques, Environ. Sci. Pollut. Res. 30 (2023) 1562–1578, https://doi.org/10.1007/s11356-022-22277-5.

[3] C. Ruan, G. Chen, Y. Ma, C. Du, C. He, X. Liu, X. Jin, Q. Chen, S. He, Y. Huang, PVA-assisted CNCs/SiO2 composite aerogel for efficient sorption of ciprofloxacin, J. Colloid Interface Sci. 630 (2023) 544–555, https://doi.org/10.1016/j.jcis.2022.10.020.

[4] B. Wang, Q. Mo, B. Qin, L. Song, J. Li, G. Sheng, D. Shi, X. Xu, L. Hou, Adsorption behaviors of three antibiotics in single and co-existing aqueous solutions using mesoporous carbon, Environ. Res. 215 (2022) 114375, https://doi.org/10.1016/j.envres.2022.114375.

[5] D. Yanardag, G.G. Kaya, S. Edebali, Ciprofloxacin adsorption performance of Co-doped UiO-66, Appl. Organomet. Chem. 38 (2024) 1–12, https://doi.org/10.1002/aoc.7311.

[6] G. Guzel Kaya, E. Aznar, H. Deveci, R. Martínez-Máñez, Low-cost silica xerogels as potential adsorbents for ciprofloxacin removal, Sustain. Chem. Pharm. 22 (2021), https://doi.org/10.1016/j.scp.2021.100483.

[7] Z. Zhang, Y. Wang, B. Chen, C. Lei, Y. Yu, N. Xu, Q. Zhang, T. Wang, W. Gao, T. Lu, M. Gillings, H. Qian, Xenobiotic pollution affects transcription of antibiotic resistance and virulence factors in aquatic microcosms, Environ. Pollut. 306 (2022) 119396, https://doi.org/10.1016/J.ENVPOL.2022.119396.

[8] L. Qalyoubi, A. Al-Othman, S. Al-Asheh, Removal of ciprofloxacin antibiotic pollutants from wastewater using nano-composite adsorptive membranes, Environ. Res. 215 (2022) 114182, https://doi.org/10.1016/j.envres.2022.114182.

[9] S.K. Mondal, A.K. Saha, A. Sinha, Removal of ciprofloxacin using modified advanced oxidation processes: Kinetics, pathways and process optimization, J. Clean. Prod. 171 (2018) 1203–1214, https://doi.org/10.1016/j.jclepro.2017.10.091.

[10] B. Feng, Y. Zhang, W. Li, G. Che, C. Liu, A. Jv, J. Lu, W. Sun, R. Guan, Efficient photocatalytic removal of ciprofloxacin through in-situ growth of g-C3N4 on the surface of clinoptilolite, J. Phys. Chem. Solids 192 (2024) 112077, https://doi.org/10.1016/j.jpcs.2024.112077.

[11] M. Golmohammadi, H. Hanafi-Bojd, M. Shiva, Photocatalytic degradation of ciprofloxacin antibiotic in water by biosynthesized silica supported silver nanoparticles, Ceram. Int. 49 (2023) 7717–7726, https://doi.org/10.1016/j.ceramint.2022.10.261.

[12] M.E. dos Santos Soldan, E.B. Lied, I.L. Costa Junior, P.R.S. Bittencourt, I. José Baraldi, R.M. Giona, A.P. Trevisan, F.H. Passig, K.Q. de Carvalho, Optimizing ciprofloxacin removal using ion exchange resin: Exploring operational parameters and assessing toxicity, Chem. Eng. Sci. 282 (2023), https://doi.org/10.1016/j.ces.2023.119317.

[13] A.E. Gahrouei, S. Vakili, A. Zandifar, S. Pourebrahimi, From wastewater to clean water: Recent advances on the removal of metronidazole, ciprofloxacin, and sulfamethoxazole antibiotics from water through adsorption and advanced oxidation processes (AOPs), Environ. Res. 252 (2024) 119029, https://doi.org/10.1016/j.envres.2024.119029.
[14] T.D. Pham, P.T. Nguyen, T.M.N. Phan, T.D. Dinh, T.M.H. Tran, M.K. Nguyen, T. H. Hoang, A.L. Srivastav, Highly adsorptive removal of ciprofloxacin and E. coli inactivation using amino acid tryptophan modified nano-gibbsite, Environ. Res. 258 (2024) 119396, https://doi.org/10.1016/J.ENVRES.2024.119396.
[15] S. Ghosh, S. Pourebrahimi, A. Malloum, O.J. Ajala, S.S. AlKafaas, H. Onyeaka, N. D. Nnaji, A. Oroke, C. Bornman, O. Christian, S. Ahmadi, M.Y. Wani, A review on ciprofloxacin removal from wastewater as a pharmaceutical contaminant: Covering adsorption to advanced oxidation processes to computational studies, Mater. Today Commun. 37 (2023), https://doi.org/10.1016/j.mtcomm.2023.107500.
[16] M.Y. Nassar, I.S. Ahmed, M.A. Raya, A facile and tunable approach for synthesis of pure silica nanostructures from rice husk for the removal of ciprofloxacin drug from polluted aqueous solutions, J. Mol. Liq. 282 (2019) 251–263, https://doi.org/10.1016/j.molliq.2019.03.017.
[17] F. Yu, X. Bai, M. Liang, J. Ma, HKUST-1-Derived Cu@Cu(I)@Cu(II)/Carbon adsorbents for ciprofloxacin removal with high adsorption performance, Sep. Purif. Technol. 288 (2022) 120647, https://doi.org/10.1016/j.seppur.2022.120647.
[18] S. Dou, X.X. Ke, L. Bin Zhong, J.J. Fan, J. Paul Chen, Y.M. Zheng, Novel ultraporous polyimide-based hollow carbon nanofiber mat: Its polymer-blend electrospinning preparation strategy and efficient dynamic adsorption for ciprofloxacin removal, Sep. Purif. Technol. 295 (2022) 121341, https://doi.org/10.1016/j.seppur.2022.121341.
[19] T.D. Pham, T.N. Vu, H.L. Nguyen, P.H.P. Le, T.S. Hoang, Adsorptive removal of antibiotic ciprofloxacin from aqueous solution using protein-modified nanosilica, Polymers (Basel). 12 (2020), https://doi.org/10.3390/polym12010057.
[20] T.N. Vu, P.H.P. Le, T.T.T. Truong, P.T. Nguyen, T.D. Dinh, T.K. Tran, T.H. Hoang, T.D. Pham, Highly adsorptive removal of antibiotic and bacteria using lysozyme protein modified nanomaterials, J. Mol. Liq. 382 (2023) 121903, https://doi.org/10.1016/j.molliq.2023.121903.
[21] T.M.D. Le, T.D. Dinh, T.M.H. Tran, M.K. Nguyen, H. Hoang, L.K. Vu, N.D.Q. Vu, T. D. Pham, Adsorption characteristics of individual and binary mixtures of ciprofloxacin antibiotic and Cu(II) on nanosilica in water, J. Mol. Liq. 398 (2024) 124298, https://doi.org/10.1016/J.MOLLIQ.2024.124298.
[22] J. Wolska, M. Frankowski, J. Jenczyk, L. Wolski, Highly sulfonated hyper-cross-linked polymers as promising adsorbents for efficient and selective removal of ciprofloxacin from water, Sep. Purif. Technol. 343 (2024) 127147, https://doi.org/10.1016/j.seppur.2024.127147.
[23] Q. Luo, P. Liu, L. Bi, L. Shi, J. Zhou, F. Fang, Q. Lv, H. Fu, X. Li, J. Li, Selective and efficient removal of ciprofloxacin from water by bimetallic MOF beads: Mechanism quantitative analysis and dynamic adsorption, Sep. Purif. Technol. 332 (2024) 125832, https://doi.org/10.1016/j.seppur.2023.125832.
[24] P. Gutiérrez-Sánchez, A. Hrichi, J.M. Garrido-Zoido, S. Álvarez-Torrellas, M. Larriba, M. Victoria Gil, H. Ben Amor, J. García, Natural clays as adsorbents for the efficient removal of antibiotic ciprofloxacin from wastewaters: Experimental and theoretical studies using DFT method, J. Ind. Eng. Chem. 134 (2024) 137–151, https://doi.org/10.1016/j.jiec.2023.12.044.
[25] F.H. Kamgang Djioko, C.G. Fotsop, G. Kamgang Youbi, S.C. Nwanonenyi, E. E. Oguzie, C. Ada Madu, Efficient removal of pharmaceutical contaminant in wastewater using low-cost zeolite 4A derived from kaolin: Experimental and theoretical studies, Mater. Chem. Phys. 315 (2024), https://doi.org/10.1016/j.matchemphys.2024.128994.
[26] G. Abu Rumman, T.J. Al-Musawi, M. Sillanpaa, D. Balarak, Adsorption performance of an amine-functionalized MCM–41 mesoporous silica nanoparticle system for ciprofloxacin removal, Environ. Nanotechnology, Monit. Manag. 16 (2021), https://doi.org/10.1016/j.enmm.2021.100536.
[27] D.A. da Silva, E.G. de Assis, D. dos Santos, Eiras,, Efficient and reusable mesoporous silica structures for ciprofloxacin removal from water media, J. Water Process Eng. 60 (2024) 105144, https://doi.org/10.1016/j.jwpe.2024.105144.
[28] D. Lu, S. Xu, W. Qiu, Y. Sun, X. Liu, J. Yang, J. Ma, Adsorption and desorption behaviors of antibiotic ciprofloxacin on functionalized spherical MCM-41 for water treatment, J. Clean. Prod. 264 (2020) 121644, https://doi.org/10.1016/j.jclepro.2020.121644.
[29] S.S. Çok, F. Koç, A. Len, N. Gizli, Z. Dudás, The role of surface and structural properties on the adsorptive behavior of vinyl-methyl decorated silica aerogel-like hybrids for oil/organic solvent clean-up practices, Sep. Purif. Technol. 334 (2024) 125958, https://doi.org/10.1016/j.seppur.2023.125958.
[30] S. Sert Çok, F. Koç, N. Gïzlï, Lightweight and highly hydrophobic silica aerogels dried in ambient pressure for an efficient oil/organic solvent adsorption, J. Hazard. Mater. 408 (2021), https://doi.org/10.1016/j.jhazmat.2020.124858.
[31] H. Choi, H.H. Han, V.G. Parale, T. Kim, W. Park, Y. Kim, J. Kim, Y. Choi, Y.S. Bae, H.H. Park, Rigid amine-incorporated silica aerogel for highly efficient CO2 capture and heavy metal removal, Chem. Eng. J. 483 (2024) 149357, https://doi.org/10.1016/j.cej.2024.149357.
[32] V.G. Parale, H. Choi, T. Kim, V.D. Phadtare, R.P. Dhavale, K.Y. Lee, A. Panda, H. H. Park, One pot synthesis of hybrid silica aerogels with improved mechanical properties and heavy metal adsorption: Synergistic effect of in situ epoxy-thiol polymerization and sol-gel process, Sep. Purif. Technol. 308 (2023) 122934, https://doi.org/10.1016/j.seppur.2022.122934.
[33] X. Tian, J. Liu, Y. Wang, F. Shi, Z. Shan, J. Zhou, J. Liu, Adsorption of antibiotics from aqueous solution by different aerogels, J. Non. Cryst. Solids 505 (2019) 72–78, https://doi.org/10.1016/j.jnoncrysol.2018.10.033.
[34] A. Mohseni-Bandpei, A. Eslami, H. Kazemian, M. Zarrabi, T.J. Al-Musawi, A high density 3-aminopropyltriethoxysilane grafted pumice-derived silica aerogel as an efficient adsorbent for ibuprofen: Characterization and optimization of the adsorption data using response surface methodology, Environ. Technol. Innov. 18 (2020) 100642, https://doi.org/10.1016/j.eti.2020.100642.
[35] A. Lamy-Mendes, D. Lopes, A.V. Girão, R.F. Silva, W.J. Malfait, L. Durães, Carbon Nanostructures—Silica Aerogel Composites for Adsorption of Organic Pollutants, Toxics 11 (2023) 1–29, https://doi.org/10.3390/toxics11030232.
[36] M. Barczak, Amine-modified mesoporous silicas: Morphology-controlled synthesis toward efficient removal of pharmaceuticals, Microporous Mesoporous Mater. 278 (2019) 354–365, https://doi.org/10.1016/j.micromeso.2019.01.012.
[37] M. Zarrabi, High-density amine-functionalized MCM-41 derived from pumice: facile synthesis and antibiotic adsorption, Polym. Bull. 80 (2023) 12761–12786, https://doi.org/10.1007/s00289-023-04685-w.
[38] P. Hongsawat, P. Prarat, C. Ngamcharussrivichai, P. Punyapalakul, Adsorption of ciprofloxacin on surface functionalized superparamagnetic porous silicas, Desalin. Water Treat. 52 (2014) 4430–4443, https://doi.org/10.1080/19443994.2013.803795.
[39] S. Sert Çok, F. Koç, Z. Dudás, N. Gizli, The Methyl Functionality of Monolithic Silica Xerogels Synthesized via the Co-Gelation Approach Combined with Surface Silylation, Gels 9 (2023), https://doi.org/10.3390/gels9010033.
[40] Z. Dudás, A. Len, C. Ianăși, G. Paladini, Structural modifications caused by the increasing MTES amount in hybrid MTES/TEOS-based silica xerogels, Mater. Charact. 167 (2020) 33–36, https://doi.org/10.1016/j.matchar.2020.110519.
[41] Z. Dudás, E. Fagadar-Cosma, A. Len, L. Románszki, L. Almásy, B. Vlad-Oros, D. Dascalu, A. Krajnc, M. Kriechbaum, A. Kuncser, Article improved optical and morphological properties of vinyl-substituted hybrid silica materials incorporating a Zn-metalloporphyrin, Materials (Basel). 11 (2018), https://doi.org/10.3390/ma11040565.
[42] P. Shajesh, S. Smitha, P.R. Aravind, K.G.K. Warrier, Synthesis, structure and properties of cross-linked R(SiO1.5)/SiO2 (R = 3-glycidoxypropyl) porous organic inorganic hybrid networks dried at ambient pressure, J. Colloid Interface Sci. 336 (2009) 691–697, https://doi.org/10.1016/j.jcis.2009.04.023.
[43] S. Sert Çok, N. Gizli, Microstructural properties and heat transfer characteristics of in-situ modified silica aerogels prepared with different organosilanes, Int. J. Heat Mass Transf. 188 (2022) 122618, https://doi.org/10.1016/j.ijheatmasstransfer.2022.122618.
[44] Z. Li, S. Zhao, M.M. Koebel, W.J. Malfait, Silica aerogels with tailored chemical functionality, Mater. Des. 193 (2020) 108833, https://doi.org/10.1016/j.matdes.2020.108833.
[45] X. Zhang, Y. Wu, S. He, D. Yang, Structural characterization of sol-gel composites using TEOS/MEMO as precursors, Surf. Coatings Technol. 201 (2007) 6051–6058, https://doi.org/10.1016/j.surfcoat.2006.11.012.
[46] N. Hüsing, U. Schubert, K. Misof, P. Fratzl, Formation and Structure of Porous Gel Networks from Si(OMe)4 in the Presence of A(CH2)nSi(OR)3 (A = Functional Group), Chem. Mater. 10 (1998) 3024–3032, https://doi.org/10.1021/cm980706g.
[47] F. Bauer, R. Mehnert, UV curable acrylate nanocomposites: Properties and applications, J. Polym. Res. 12 (2005) 483–491, https://doi.org/10.1007/s10965-005-4339-z.
[48] X. Ji, J.E. Hampsey, Q. Hu, J. He, Z. Yang, Y. Lu, Mesoporous silica-reinforced polymer nanocomposites, Chemistry of Materials 15 (19) (2003) 3656–3662.
[49] T. Shimizu, K. Kanamori, A. Maeno, H. Kaji, C.M. Doherty, P. Falcaro, K. Nakanishi, Transparent, Highly Insulating Polyethyl- and Polyvinylsilsesquioxane Aerogels: Mechanical Improvements by Vulcanization for Ambient Pressure Drying, Chem. Mater. 28 (2016) 6860–6868, https://doi.org/10.1021/acs.chemmater.6b01936.
[50] N. Hüsing, F. Schwertfeger, W. Tappert, U. Schubert, Influence of supercritical drying fluid on structure and properties of organically modified silica aerogels, J. Non. Cryst. Solids 186 (1995) 37–43, https://doi.org/10.1016/0022-3093(95)00031-3.
[51] P. Innocenzi, A. Sassi, G. Brusatin, M. Guglielmi, D. Favretto, R. Bertani, A. Venzo, F. Babonneau, A novel synthesis of sol-gel hybrid materials by a nonhydrolytic/hydrolytic reaction of (3-glycidoxypropyl)trimethoxysilane with TiCl4, Chem. Mater. 13 (2001) 3635–3643, https://doi.org/10.1021/cm011034o.
[52] P. Innocenzi, G. Brusatin, F. Babonneau, Competitive polymerization between organic and inorganic networks in hybrid materials, Chem. Mater. 12 (2000) 3726–3732, https://doi.org/10.1021/cm001139b.
[53] S. Rezaei, A.M. Zolali, A. Jalali, C.B. Park, Strong, highly hydrophobic, transparent, and super-insulative polyorganosiloxane-based aerogel, Chem. Eng. J. 413 (2021) 127488, https://doi.org/10.1016/j.cej.2020.127488.
[54] A. Len, G. Paladini, L. Románszki, A.M. Putz, L. Almásy, K. László, S. Bálint, A. Krajnc, M. Kriechbaum, A. Kuncser, J. Kalmár, Z. Dudás, Physicochemical characterization and drug release properties of methyl-substituted silica xerogels made using sol–gel process, Int. J. Mol. Sci. 22 (2021) 1–23, https://doi.org/10.3390/ijms22179197.
[55] G. Beaucage, Small-angle scattering from polymeric mass fractals of arbitrary mass-fractal dimension, J. Appl. Crystallogr. 29 (1996) 134–146, https://doi.org/10.1107/S0021889895011605.
[56] G. Guzel Kaya, E. Aznar, H. Deveci, R. Martínez-Máñez, Low-cost silica xerogels as potential adsorbents for ciprofloxacin removal, Sustain. Chem. Pharm. 22 (2021) 100483, https://doi.org/10.1016/J.SCP.2021.100483.
[57] W.R.D.N. Sousa, A.R. Oliveira, J.F. Cruz Filho, T.C.M. Dantas, A.G.D. Santos, V.P. S. Caldeira, G.E. Luz, Ciprofloxacin Adsorption on ZnO Supported on SBA-15, Water, Air. Soil Pollut. 229 (2018), https://doi.org/10.1007/s11270-018-3778-1.
[58] Z. Liang, Z. Zhaob, T. Sun, W. Shi, F. Cui, Adsorption of quinolone antibiotics in spherical mesoporous silica: Effects of the retained template and its alkyl chain

length, J. Hazard. Mater. 305 (2016) 8–14, https://doi.org/10.1016/J.JHAZMAT.2015.11.033.
[59] C.A. Igwegbe, S.N. Oba, C.O. Aniagor, A.G. Adeniyi, J.O. Ighalo, Adsorption of ciprofloxacin from water: A comprehensive review, J. Ind. Eng. Chem. 93 (2021) 57–77, https://doi.org/10.1016/j.jiec.2020.09.023.
[60] L. Gabrielli, L. Russo, A. Poveda, J.R. Jones, F. Nicotra, J. Jiménez-Barbero, L. Cipolla, Epoxide opening versus silica condensation during sol-gel hybrid biomaterial synthesis, Chem. - A Eur. J. 19 (2013) 7856–7864, https://doi.org/10.1002/chem.201204326.
[61] X. Peng, F. Hu, T. Zhang, F. Qiu, H. Dai, Amine-functionalized magnetic bamboo-based activated carbon adsorptive removal of ciprofloxacin and norfloxacin: A batch and fixed-bed column study, Bioresour. Technol. 249 (2018) 924–934, https://doi.org/10.1016/j.biortech.2017.10.095.
[62] F. Parsaee, M.C. Senarathna, P.B. Kannangara, S.N. Alexander, P.D.E. Arche, E. R. Welin, Radical philicity and its role in selective organic transformations, Nat. Rev. Chem. 5 (2021) 486–499, https://doi.org/10.1038/s41570-021-00284-3.
[63] A. Irfan, A.G. Al-Sehemi, A. Kalam, Tuning the Electronic and Charge Transport Properties of Schiff Base Compounds by Electron Donor and/or Acceptor Groups, Materials (Basel). 15 (2022), https://doi.org/10.3390/ma15238590.
[64] F. Yu, Z. Yang, X. Zhang, P. Yang, J. Ma, Lanthanum modification κ-carrageenan/sodium alginate dual-network aerogels for efficient adsorption of ciprofloxacin hydrochloride, Environ. Technol. Innov. 24 (2021) 1–13, https://doi.org/10.1016/j.eti.2021.102052.
[65] S.H. Wang, P.R. Griffiths, Resolution enhancement of diffuse reflectance ir spectra of coals by Fourier self-deconvolution: 1. CH stretching and bending modes, Fuel 64 (2) (1985) 229–236.
[66] Z. Li, H. Hong, L. Liao, C.J. Ackley, L.A. Schulz, R.A. Macdonald, A.L. Mihelich, S. M. Emard, Colloids and Surfaces B : Biointerfaces A mechanistic study of ciprofloxacin removal by kaolinite, Colloids Surfaces B Biointerfaces 88 (2011) 339–344, https://doi.org/10.1016/j.colsurfb.2011.07.011.
[67] S. Rakshit, D. Sarkar, E.J. Elzinga, P. Punamiya, R. Datta, Mechanisms of ciprofloxacin removal by nano-sized magnetite, J. Hazard. Mater. 246–247 (2013) 221–226, https://doi.org/10.1016/j.jhazmat.2012.12.032.